

DYNAMICS OF CONTACT SURFACES UNDER PURE ROLLING AND ROLLING WITH TRACTION

THIS THESIS HAS BEEN ACCEPTED FOR
THE DEGREE OF..... *MSc. 1994*.....
AND A COPY MAY BE PLACED IN THE
UNIVERSITY LIBRARY.

By

Odhiambo. V.

**A Thesis submitted to the University of
Nairobi in partial fulfilment for the
degree of Masters of Science in
Mechanical Engineering**

University of NAIROBI Library




0404592 8

October 1994


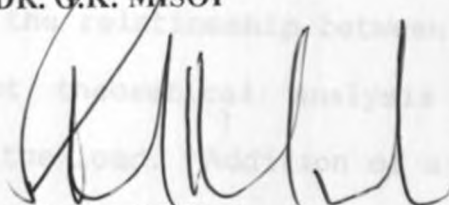
DECLARATION

**THIS THESIS IS MY ORIGINAL WORK AND HAS NOT BEEN PRESENTED FOR A
DEGREE IN ANY OTHER UNIVERSITY**


ODHIAMBO V. 15/7/96

**THE THESIS HAS BEEN SUBMITTED FOR EXAMINATION WITH MY APPROVAL
AS**

THE UNIVERSITY SUPERVISOR


DR. G.K. MISOI

DR. S.M. MUTULI 25/7/96

**DEPARTMENT OF MECHANICAL ENGINEERING
UNIVERSITY OF NAIROBI**

ABSTRACT

Formation of intermittent profiles of constant wavelength usually referred to as corrugation on rolling surfaces has been a major problem in industry. Corrugation result in vibration, noise, overstressing and finally failure of components at the peak dynamic stresses.

The natural contact frequency often matches the intermittent wear wavelength produced on rolling surfaces but the effects of the dynamical parameters on it have not been quantitatively established. The study investigated their contribution on corrugation.

In the study it was found that the corrugation forms between a certain contact load range within which the wavelength is proportional to the rolling speed . It was not possible to establish experimentally the relationship between the wavelength and the radial load but theoretical analysis showed slight decrease with increase of the load. Addition of a tractive force to the contact complicated the Hertzian analysis and it lowered the dynamic limits.

ACKNOWLEDGEMENTS

I am grateful to the lecturers in the department of Mechanical Engineering of the University of Nairobi who guided me during the course of this work. My special gratitude goes to Dr.G.K. Misoi and Dr. S.M. Mutuli for their keen supervision and assistance which made the research work to be completed in time.

I am thankful to the Kenya Railways Corporation for the financial support which enabled me to carry out the work contained in this thesis and for the use of their various specialized machines and facilities at the Central Workshops. I am also indebted to the staff in Metrology Department of the Kenya Bureau of Standards for their lucid instruction in the techniques used to analyse the profiles of the worn surfaces.

Finally I wish to express my gratitude to the technical staff of the Laboratory, Mechanical Engineering, especially Mr.Calleb for his assistance in construction of the corrugation rig used in this research project.

TABLE OF CONTENTS

	CHAPTER ONE	PAGE
	1. INTRODUCTION	1
1.1	Corrugation	2
1.2	Thesis layout	3
	CHAPTER TWO	
	2. LITERATURE REVIEW	4
2.1	Definition of frictional wear and wear mechanisms	4
2.1.1	Adhesive wear	4
2.1.2	Abrasive wear	5
2.1.3	Surface fatigue wear	5
2.1.4	Fretting wear	6
2.1.5	Delamination wear	7
2.2	Frictional wear and mechanical properties	7
2.3	Intermittent Wear	9
2.4	Corrugation on railway tracks	10
2.5	Intermittent wear and the system dynamics	11

	PAGE
2.6 Hertz's contact theory	14
2.6.1 Hertz's analysis	15
2.6.2 The shape of the contact area	17
2.7 Radial stiffness of the contact	21
2.7.1 For line contacts	22
2.7.2 For circular point contacts	23
2.7.3 For elliptical point contacts	24
2.8 Longitudinal stiffness of the contact	27
2.9 Sliding as one of the sources of resistance to rolling	33
2.10 The effect of tractive force on the contact pressure distribution	34
2.11 The scope of the thesis	35
 CHAPTER THREE 	
3. EXPERIMENTAL APPARATUS	37
3.1 The rolling rig	37
3.1.1 Contact geometry	38

	PAGE
3.1.2 Upper arm size	39
3.1.3 Bearing type	40
3.1.4 Wear and corrugation test materials	40
3.2 Contact frequency	41
3.3 The contact load	42
3.4 The loading spring	43
3.5 Forced excitation of the stationary discs and the response recording units	45
3.6 The motor drive unit	47

CHAPTER FOUR

4. EXPERIMENTAL PROCEDURE	57
4.1 Calibration of the loading bolt turns	57
4.2 Determination of the approach of distant points with the radial contact force	58
4.3 Plastic initiation contact forces	60
4.4 System resonances with the rollers stationary	61
4.5 The rolling tests	62

CHAPTER FIVE

5. RESULTS

64

CHAPTER SIX

6. DISCUSSION

80

6.1	The mathematical model	80
6.2	Pivoted arm resonance due to the loading spring	82
6.3	Plastic deforming load estimations	83
6.4	Contact stiffness	86
6.5	Expected contact resonance	88
6.6	Dynamic corrugation calculations	89
6.7	The radial vibration modes	92
6.8	The loading spring stiffness	96
6.9	Relationship between the approach of distant points and the radial contact load	97
6.10	Roll Vibration of the pivoted arm due to the contact stiffness between the surfaces	100

	PAGE
6.11 System resonanse with the stationary rollers	101
6.12 General observations on the rolling tests	102
6.12.1 Corrugation wavelength and the rolling speed	105
6.12.2 Corrugation wavelength and the contact force	107
6.12.3 Rolling wear and the lateral movements	109
6.12.4 Intermittent wear and the tractive force	110
6.13 Corrugation and the metallurgical properties	111
6.14 The prifiles of the corrugated surfaces	112

CHAPTER SEVEN

7. CONCLUSIONS	114
----------------	-----

CHAPTER EIGHT

8. RECOMMENDATIONS	118
--------------------	-----

9. REFERENCES	119
---------------	-----

APPENDIX	125
----------	-----

LIST OF FIGURES

FIG. 2.1	Contact made by two bodies with non-conforming surfaces subjected to a compressive force	16
2.2	The general shape of Hertzian contact region	21
2.3	Tangential surface tractions which arise from a combination of normal and tangential forces which do not cause the bodies to slide relative to each other	27
2.4	Contact of cylinders with their axes parallel. Surface tractions due to a tangential force $Q < \mu P$. Curve A- no slip, Curve B- partial slip.	28
2.5	Curve of variation of tangential stiffness with tractive force	32

2.6	Schematic diagram of principal stresses on surfaces of cylinders loaded both radially and tangentially	34
FIG.3.1	Dynamics of a rolling contact system	37
3.2	Edge contact between cylinders formed as a result of bearing misalignment	38
3.3	Views of the toroid	49
3.4	Front view of the rolling rig showing the main assemblies 1, 2 and 3	50
3.5	Pivot assembly	51
3.6	Disc mounting assembly	52
3.7	Crowned disc housing assembly	53
FIG. 4.1	Arrangement of the rolling rig for experimental determination of the approach of distant points on the rollers with the radial force	60

FIG. 5.1(a)	Plot of log P against log delta for aluminium	69
(b)	Plot of log P against log delta for steel disc	70
(c)	Plot of log P against log delta for perspex	71
(d)	Plot of log P against log delta for the various test discs	72
5.2(a)	Plot of radial stiffness against contact force for aluminium	73
FIG. 5.2(b)	Plot of radial stiffness against contact force for the test discs	74
5.3	Plot of vibration frequency of the pivoted arm against contact force	75
5.4(a)	Response plot for perspex loaded at 250 N	76
(b)	Response plot for steel disc loaded at 500 N	77
(c)	Response plot for aluminium loaded at 750 N	78
5.5	The profiles of the corrugated surfaces	79

	PAGE
FIG. 6.1 Rolling discs arrangement for studying radial dynamics of a rolling contact	80
6.2 Loading spring induced vibrations on the pivoted arm	82
6.3 Effective mass of the pivoted arm suspended by the contact "spring" of the Hertzian zone of the rolling discs	88
6.4 Representation of the radial vibration of rolling system	93

LIST OF TABLES

TABLE 5.1 Loading spring compressions with load and computations for the calculation of the axial stiffness	64
5.2 Experimental and theoretical plastic initiation loads for various 20 mm thick roller material test pieces	65

TABLE 5.3	Response of a forced excitation of the loaded contacts	66
5.4	Experimental and theoretical corrugation wavelengths on selected roller test pieces loaded at 700 N and pure rolled at various speeds.	67
5.5	The dynamic loading ranges of various discs when purely rolled and when rolled with tractive forces	67
5.6	Expected corrugation wavelengths on steel test discs rolled at 400 r.p.m. under different contact loads	68
TABLE 6.7	Summary of the observations made on the surfaces of aluminium test discs whose free rollings were prevented by the application of braking forces to the crowned disc.	68

LISTS OF PLATES

PLATE 3.1	The motor and the gear box assembly	54
3.2	The pivoted arm assembly	54
3.3	The rolling rig	55
3.4	The test disc holder	55
3.5	Some of the corrugated test discs	56

NOTATION

SYMBOL	DESCRIPTION	UNITS
a	Semi-major axis of the projected contact zone	m
b	Semi-minor axis of the projected contact zone	m
B.H.N.	Brinell hardness number	
A, B, C ₁	Numerical constants	
δ	Radial approach of distant points	μm
e	Numerical constant	
E	Modulus of elasticity	N m ⁻²
E*	Plane modulus of elasticity	N m ⁻²
E _r	Reduced modulus of elasticity	N m ⁻²

SYMBOL	DESCRIPTION	UNITS
f	Vibrational frequency	Hz.
f_n	Natural frequency	Hz.
F	Frictional force	N
g	Acceleration due to gravity	$m\ s^{-2}$
G	Shear modulus of elasticity	$N\ m^{-2}$
h	Separation of distant points	m
k	Shear flow stress of a material	$N\ m^{-2}$
K_i	Stiffness	$N\ m^{-1}$
K_s	Spring axial stiffness	$N\ m^{-1}$
K_h	Linearized Hertzian contact stiffness	$N\ m^{-1}$
l_i	Length	m
μ	Coefficient of friction	
m_i	Mass	Kg
N	Rotational speed	r.p.m
π	Numerical constant	
p	Hertzian contact pressure	$N\ m^{-2}$

SYMBOL	DESCRIPTION	UNITS
p_0	Max. contact pressure	$N\ m^{-2}$
P	Normal contact force	N
q	Tangential stress near the point of contact	$N\ m^{-2}$
q_0	Max. shear stress	$N\ m^{-2}$
Q	Tractive force	N
ρ	Density	$Kg\ m$
r	Radial coordinate	m
R	Radius of curvature	m
ω	Angular velocity	$Rad.s^{-1}$
w	Width of the contact zone	m
ν	Poisson's ratio	
Θ	Angular coordinate	$Rad.$
ϕ	Phase angle	$Rad.$
x, y, z	Cartesian coordinates	m

1. INTRODUCTION

The studies of the characteristics of the failure of machines and mechanisms have shown that in 75% of cases, failure occurs due to the wear of rubbing surfaces, Kragelsky, [1982]. Accordingly, increasing the wear resistance of machine components is one of the ways of enhancing their life. However, it is impossible to extend durability of rolling or rubbing parts of machines without establishing the physico-mechanical characteristics of the materials and the conditions of operation of the sliding or rolling system, i.e.

- the contact load
- the sliding or rolling speed
- the design features of the contacts
- the dynamics of the contact surfaces and
- the surface conditions such as lubrication and other environmental factors.

Rolling contacts are designed to reduce friction and hence, surface wear by replacing sliding friction with rolling friction Nippon, [1978]. Rolling friction causes small power loss, reduce surface temperature and allows high speed operation. It also ensure

increased accuracy and reliability of machines. With rolling surfaces, however, it is impossible to completely eliminate sliding contact because of their types and structure and as a result so many articles, Nippon, [1978] have been written on the contribution of the bearing load, finish accuracy of the contact surfaces, metallurgical properties and type and extent of lubrication applied to the sliding surface.

1.1 Corrugation

When two bodies are rolling with a contact pressure between them there will exist a material dilatation (volumetric loss) brought about by either material removal (wear), material redistribution or both at different points along the surface causing uneven surface deformation with a constant wavelength known as corrugation, Mulvaney, [1986].

Surface deformation, which results in the formation of corrugations whose wavelengths are associated with the dynamic characteristics of the contact is predicted to be a plastic change of the weaker material as it is subjected to peak loads exceeding the yield point of the material as the rolling bodies oscillate radially due to the elastic contact between the elastically loaded regions of the surfaces.

1.2 Thesis layout

In this thesis the relevant facts about the study of dynamics of contact surfaces under pure rolling and rolling with traction is presented. It is divided into eight chapters, the introduction being the first one. Chapter two contains the review of the literature required for sound understanding of the study problem. In that chapter corrugation and other surface wear modes are explained and the factors influencing their formation documented.

The study required the fabrication of a rolling rig to simulate the actual rolling surfaces. The characteristics of the rig is described in chapter three. The procedure on how both the static and rolling tests and the results obtained are contained in chapters four and five respectively. There was a great agreement between the experimental results and the theoretical predictions showing that the formation of intermittently worn surfaces on rolling bodies is indeed a dynamic phenomenon. Those and other findings are contained in chapters six, seven and eight.

2. LITERATURE REVIEW

2.1 Definition of frictional wear and wear mechanisms

Wear is a process in which the surface layers of a solid are ruptured as a result of the mechanical action of another body or medium. If the mechanical action appears in the form of friction forces, this is called frictional wear. This is the type of wear under which rolling surface wear is categorised. According to Engel [1976] other forms of frictional wear are adhesive wear, abrasive wear, surface fatigue wear, fretting wear, and delamination wear.

2.1.1 Adhesive wear

Adhesive friction wear may be explained by the molecular attractions existing between two relatively moving materials. It is evident that the smoother the surfaces the larger the adhesion between the surfaces thus an adhesive friction mechanism works contrary to the erroneous classical idea equating smoothness with the absence of friction. When adhesive wear forms, atoms or clusters of atoms, are removed from the junctions by virtue of their adhesive junction strength becoming larger than the cohesive strength of the material.

2.1.2 Abrasive wear

A source of friction wear of sliding bodies may be the resistance offered by interlocking asperities of the interface. This is often termed abrasive wear. There are two types of abrasive wear:

- i) Two-body abrasive wear occurring when a hard and rough body plough into a softer body and
- ii) Three-body abrasive wear found when a third agent, usually hard, granular matter, is placed between the sliding surfaces, and gets embedded into one of the surfaces, and cuts grooves in the opposite one.

A common utilization of two-body abrasive wear is found in filling process; three-body abrasive wear is the basis of polishing.

Wear kinetics as studied by Mathia [1992] has improved the understanding of this wear process during sliding, and helped in identifying the optimum topography and manufacturing procedure leading to desired sliding functions and the specific criteria of morphologies.

2.1.3 Surface fatigue wear

Surface fatigue wear is caused by cyclic loads at relatively medium stresses. It is related to stress hysteresis of the surface layer

and, until quite recently has been generally considered only in rolling contacts. Rolling elements, subjected to repetitive cycles of a Hertz-type contact stress develop sub-surface cracks which eventually lead to a spalling-type failure. This mode of failure was found to be highly stress-dependent by Lundre and Palmgren [1956] who empirically established the equation

$$P' N = \text{constant} \quad (2.1)$$

where N denotes the number of cycles to failure at load P and constant geometry.

2.1.4 Fretting wear

Fretting wear is caused by the small amplitude tangential oscillation of contacting surfaces and may arise inspite of lubrication, and on diverse materials such as glass, wood, jewels and gold. Whereas in ordinary sliding debris can readily escape, fretting tends to keep it around contact. Slip amplitudes of the orders of 10 μ m and very low speed vibrations, Engel, [1976] have been observed to cause fretting wear. The latter may result in a severe cleaning action if relubrication of the surface is prevented.

2.1.5 Delamination wear

In 1973, Suh advanced a new theory, Suh [1973] of metallic sliding wear based on metallurgical observation of several sliding materials. He observed that wear mechanism manifested itself through the delamination of the surface into thin wear sheets parallel to the surface. By sectioning wear scars normal to the surface, Suh and his team at the Massachusetts Institute of Technology observed far greater damage in the subsurface layers than in the layers closest to the surface. This is attributed to less cold working in the surface layers, enabling it to absorb plastic deformation.

2.2 Frictional wear and mechanical properties

An attempt to relate wear to the mechanical properties of materials was made by Tonn in 1937, who proposed an empirical formula for abrasive wear. Later, in 1940, Holm [1946] using the atomic mechanism of wear as his starting point, calculated the volume of substance worn over unit sliding path, i.e.,

$$W = Z (N / B) \quad (2.2)$$

where W is the wear rate,

Z is the probability of removing a cluster of atoms from the surface when it encounters one of the opposite member,

N is the load and

B is Brinell hardness of material.

The American scientists Burwell and Strang [1952] in 1952 developed an adhesion theory of wear, and proposed a theoretical equation identical in structure with Holm's equation. They considered that micro-volumes of material are removed during wear.

Archard [1953] on the assumption that wear particles are hemispherical with radius equal to the radius of a contact point, showed that

$$W = k N / (3B) \quad (2.3)$$

where

k is the probability of removing a wear particle from the contact point.

The next important stage in the development of wear theory was the emergence of the fatigue theory for the wear of solids proposed in the USSR. A paper on this theory was published by Kragelsky in 1957. This theory incorporates the concept of an individual frictional bond deformed by the bulk of the rubbing bodies, the stress distribution of this volume as a function of the load, and the geometrical profile of the microasperities is considered. The type of stress distribution determines the way in which the frictional bonds are distributed. The main concept of this theory is that destruction of sliding surface

requires repeated sliding effects; the number of which can be expressed quantitatively as a function of the stress distribution.

2.3 Intermittent wear

Intermittent wear on rollers of a rolling disc machine may be attributed to the resonance of the rig itself and also of the excitation of the contact by irregularities on either the rolling surfaces the rig assembly with a consequential periodic deformation of the surfaces and propagation of the corrugations with the subsequent rolling of the rollers. Other areas where this form of wear takes place are in metalworking processes such as machining on lathe and grinding, on railway tracks, on races of ball and roller bearings, on rollers of steel rolling mills, and in paper industry where it is encountered as "barring" of the newsprint, Grassie [1979].

"Chatter" of the machine tools results in the formation of uneven surfaces due to vibration of the machines. These vibrations are usually self-excited vibrations, which have a frequency equal to that of the resonance of the system, (the machine tool, workpiece and tool). When account is taken of the contact stiffness between the tool and workpiece Cockerham and Symmons [1976] have proposed a mathematical model for analysing chatter, and have found that stick-slip of the machine tool can be eliminated if sufficient damping is incorporated in the system.

Barring of newsprint in paper industry is apparent as glossy transverse lines occurring at regular intervals of 10-150 mm, Grassie [1979]. Such bars are the manifestation of a varying thickness of the paper while the density of the paper varies in inverse proportion to its thickness. It has been shown by Parker [1965] that barred paper is a consequence of differential wear of the rollers between which the paper passes as it is rolled to the desired thickness.

2.4 Corrugations on railway tracks

Corrugations of railway tracks was first reported in "The Engineer" of 1904, though the problem was already an old one. These surface deformations on rails are as a consequence of the phenomenon of contact vibration. Such vibrations arise from the rail joints or any other pre-existing roughness of the rail, while wavelength of the corrugation is determined by the frequency of that mode in which the effective masses of the locomotive and the rail foundation vibrate in antiphase on the flexibility which results from the local deformation of the bodies at their point of contact. It has been demonstrated that rail corrugations could be suppressed by introducing sufficient damping in the contact mode of vibration.

It has also been recognised that the high-pitched squeal on railway wheels transversing tight curves is an outcome of the wheel

periodically sticking and slipping. Bugacis [1973] observed that a considerable reduction in such noise had been effected on the railway in Humburg by adopting aluminium, and relatively well-damped plastic coated steel wheels. Halling [1985] has also been able to design rolling contacts operating in adverse conditions using a thickness of soft metal coating enhancing elasticity at the contacts.

2.5 Intermittent wear and the system dynamics

Intermittent wear or corrugation is a common problem on railway tracks, where the noise produced by passing wheels has led to the name "roaring rails". This phenomenon is economically important for corrugation leads to vibration, to noise, and to overstressing and the only known cure is to level the surface by grinding the rail. Previous researchers working on intermittent wear have contributed as follows:

Carson [1970] in his work on rolling disc machine found that when the wavelength of the corrugation is greater than the width of the contact region, periodic corrugations result. However, if the contact width is greater than the wavelength, rippling of random roughness results. He pointed out the fact that if a wave corrugation has to form material must move. His problem, therefore, was to determine the mechanism by which this is achieved and the possibilities he came up with were;

wear, which removed material from the surface, and plastic deformation, which redistributed it within the surface.

Carson and Johnson [1971] found that discs, when mounted on a rolling contact disc machine, show strong contact resonance. Two types of self generated corrugations were observed in the rolling rig, namely; by plastic deformation and "stick-slip" wear process. They observed that plastic corrugations developed with or without sliding and with or without lubricant while wear corrugations required a sliding motion in addition to rolling. Brass discs, on one hand, with or without sliding, in contact with a hard steel disc developed corrugations by plastic indentation which spread progressively from an irregularity in the surface. Duralumin discs, on the other hand, rolling, with sliding, in the absence of a lubricant developed severe corrugations by "stick-slip" process. In both cases the observed frequency corresponded to the frequency of contact resonance.

Both types of corrugations developed more readily with positive sliding, i.e., with the test disc moving faster than the mating disc, and less readily with negative sliding. Plastic deformations were initiated by plastic indentation in the surface which occurred spontaneously due to random dynamical overloads excited by the manufacturing irregularities on the disc surface. Measured wavelength and surface velocity corresponded to the "corrugation frequency" which was found to be less than the contact resonance frequency. This they

noted, was due to non-linearity in the system introduced by severe vibrations which caused the disc to bounce out of contact.

Gray and Johnson [1972] carried out a study on solid rollers pressed into contact on a rolling contact disc machine to simulate a wheel and a track. They noted that vibrations cause the contact force to fluctuate with various possible outcomes. Severe vibrations could cause the mating surfaces to bounce out off the contact and thereby influence the frictional forces between the wheel and the rail, which provide propulsion, braking and lateral guidance. At the same time the maximum value of the dynamic contact force could exceed the elastic limit of the metallic materials resulting in permanent indentation of the surface. They observed that contact load and damping were significant parameters in corrugation formation.

A few years later they observed that metallic corrugations originate from pre-existing irregularities in the surface, in the form of step or random surface roughness, arising from the method of manufacture. They found that the wavelength of the corrugations was determined by the frequency of contact resonance, i.e., the mode of vibration in which the rolling bodies are coupled by the elastic deformation in their contact region. Observation was made that steady load, damping of the system and the surface roughness govern the formation of corrugations. The amplitude of these corrugations stabilized after a significant number of passes and there existed a lower limit of speed below which corrugations did not form. This occurred when the expected

wavelength became comparable with the width of the contact area. The development of a corrugated surface was found to be a progressive process which took many cycles of rolling contact. However, when damping was low and contact load was high, the vibrations were severe enough to cause plastic indentation of the surface in one revolution.

2.6 Hertz's contact theory

A contact is said to be conforming if the surfaces of the two bodies "fit" exactly or closely together without deformation. Flat slider bearings and journal bearings are examples of conforming contacts. Bodies which have dissimilar profiles are said to be non-conforming. When brought into contact without deformation they will touch first at a point -"point contact"- for example, in a ball-bearing the balls make point contacts with the races, whereas in a roller bearing the rollers make line contacts. Line contact arises when the profiles of the bodies are conforming in one direction and non-conforming in the perpendicular direction.

The contact area between non-conforming bodies is generally small compared with the dimensions of the bodies themselves; the stresses are highly concentrated in the region close to the contact zone and are not greatly influenced by the shape of the bodies at a distance from the contact area.

2.6.1 Hertz's analysis

On the application of a compressive force to non-conforming surfaces the contact area, which will be generally small compared with the dimensions of the bodies will, change from being a point or a line into a shape and size dependent on the force, material properties and the geometry of the bodies at the point of contact. The contact area, shape, and stress distribution in the zone formed by two non-conforming surface profiles are best determined by Hertz's [1895] analysis which require the following assumptions to be made:

- i) Each surface is considered to be topographically smooth on both micro and macro scale. On the micro scale this implies the absence or disregard of small surface irregularities which would lead to discontinuous contact highly local variations in the contact pressure. On the macro scale the profiles of the surfaces are continuous up to their second derivatives in the contact region. This enables us to express the separations of points close to the point of contact by the expression

$$h = A x^2 + B y^2 \quad (2.4)$$

where A and B are constants with x and y being the axes on the plane normal to which the separation h is defined as shown in figure 2.1.

- ii) The dimensions of the contact zone are small in comparison with those of the bodies themselves.
- iii) The stresses are highly concentrated in the region close to the contact zone and are not greatly influenced by the shape of the bodies at a distance from the contact zone.
- iv) The bodies are perfectly elastic.

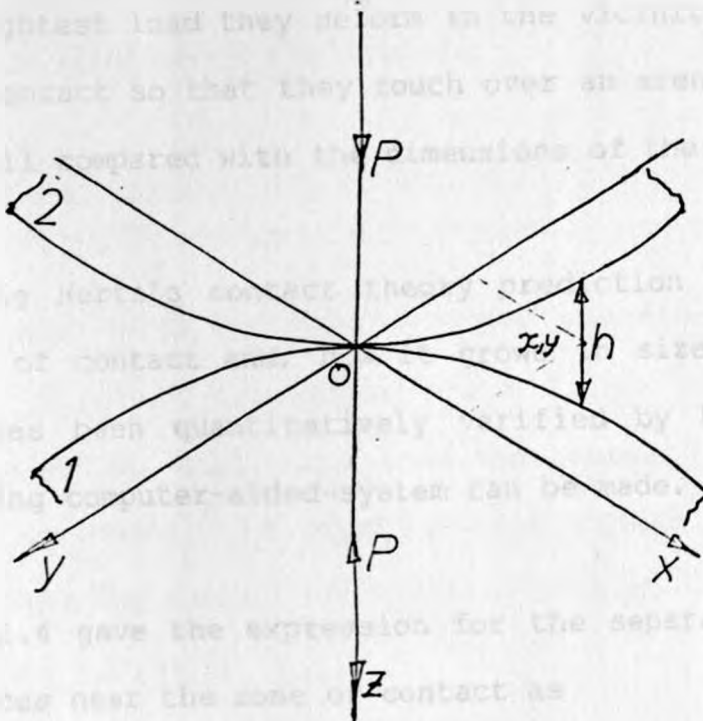


Fig. 2.1 Contact made by two bodies with non-conforming surfaces subjected to a compressive force.

The Hertzian assumptions will apply in this application and for simplification of the theoretical analysis either the contact of two spheres or two thin discs can be considered; all the arguments would then be extended to cover the more general case of a toroid and a cylinder contact on which the experiment was done.

2.6.2 The shape of contact area

When two non-conforming solids are brought into contact they touch initially at a single point or a line. Under the action of the slightest load they deform in the vicinity of their point of first contact so that they touch over an area which is finite though small compared with the dimensions of the two bodies.

By applying Hertz's contact theory prediction of the shape of this area of contact and, how it grows in size with increasing load as has been quantitatively varified by Babus'qaq, et al [1992] using computer-aided-system can be made.

Equation 2.4 gave the expression for the separation between the two surfaces near the zone of contact as

$$h = A x^2 + B y^2 \quad \text{where } A \text{ and } B \text{ are constants}$$

related to the principal relative radii of curvature R' and R''

of the bodies. If α is the angle between the axes of the bodies then according to Johnson [1985] and Appendix 1 we have

$$A + B = 0.5 (1/R'_1 + 1/R''_1 + 1/R'_2 + 1/R''_2) \quad (2.5a)$$

and

$$B - A = 0.5 \sqrt{[(1/R'_1 - 1/R''_1)^2 + (1/R'_2 - 1/R''_2)^2 + 2(1/R'_1 - 1/R''_1)(1/R'_2 - 1/R''_2)\cos 2\alpha]} \quad (2.5b)$$

It should be noted that R' and R'' being the principal radii of curvature of the surface at the origin are the minimum and maximum values respectively of the radius of curvature of all possible cross-section of the profile.

Case 1 (General Case)

In the general case it follows from equation 2.4 that the contours of constant separation are ellipses in plan. It is therefore expected, that under load the contact surface would be elliptical in shape. A special case arises when two equal cylinders both of radius R are in contact with their axes perpendicular ($\alpha = \Pi/2$); here

$$\text{min. radius of curvature} \quad R'_1 = R'_2 = R$$

$$\text{max. radius of curvature} \quad R''_1 = R''_2 = \infty$$

from which

$$A + B = 0.5 (1/R + 0 + 1/R + 0) = 1/R$$

$$A = 1/R - B \quad (2.6)$$

$$B - A = 0.5 \sqrt{(1/R^2 + 1/R^2 - 2/R^2)} = 0$$

i.e.,

$$A = B \quad (2.7)$$

Equating equations 2.6 and 2.7 gives

$$1/R - B = B$$

or $2B = 1/R$

and

$$A = B = 1/2R \quad (2.8)$$

Therefore

$$h = (x^2 + y^2) / 2R \quad (2.9)$$

In this case the contours of constant separation are circles and identical to those due to a sphere of the same radius R in contact with a plane surface.

Case 2 (Two Cylindrical Bodies of Radii R_1 and R_2 in contact with their axes parallel to the x- axes)

Here we have

$$R'_1 = R_1 ; R''_1 = \infty ; R'_2 = R_2 ; R''_2 = \infty ; \alpha = 0 ; \text{ so that}$$

$$A + B = (1/R_1 + 1/R_2)/2$$

i.e.,

$$A = (1/R_1 + 1/R_2)/2 - B \quad (2.10)$$

and

$$B - A = \sqrt{(1/R_1^2 + 1/R_2^2 + 2/R_1R_2)}/2 = (1/R_1 + 1/R_2)/2$$

i.e.,

$$A = B - (1/R_1 + 1/R_2)/2 \quad (2.11)$$

giving

$$B = (1/R_1 + 1/R_2)/2$$

and

$$A = B - (1/R_1 + 1/R_2)/2 = 0$$

hence

$$h = (1/R_1 + 1/R_2) y^2/2 \quad (2.12)$$

Contours of constant separation are straight lines parallel to the x-axis, and when loaded, the surface will make a contact over a narrow strip parallel to the x-axis.

2.7 Radial stiffness of the contact

The size of the area of contact, the distribution of stresses upon it and the approach of two bodies are given by the expressions derived from Hertzian analysis which are available in any standard texts on Contact Mechanics, Johnson [1985]. In the general case, where the separation is given by equation 2.4, the shape of the contact area is not known with certainty in advance. However, assuming tentatively that it is elliptical in shape, having semi-axes a and b as shown in figure 2.2.

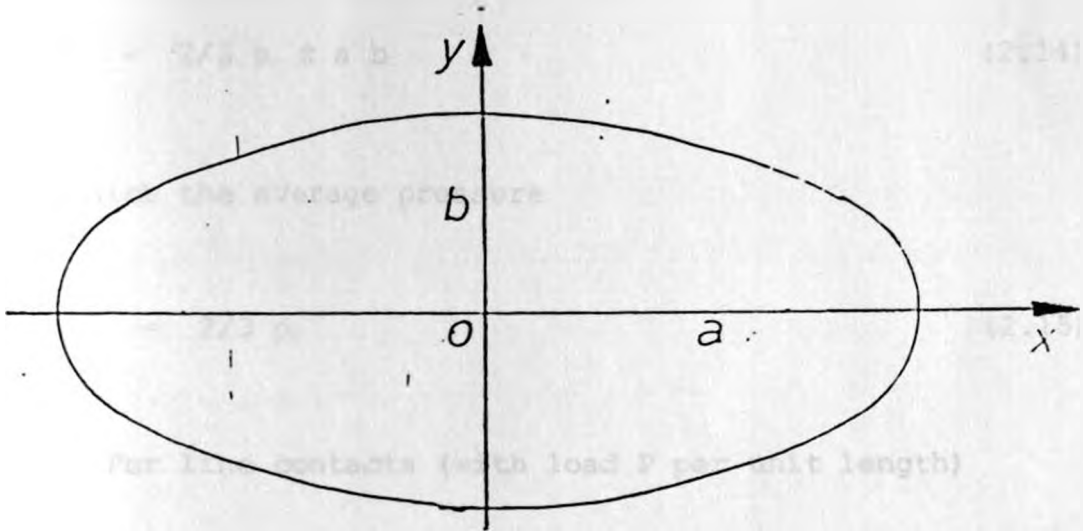


Fig. 2.2 The general shape of Hertzian contact region.

Hertz recognised that the problem in elasticity is analogous to one of electrostatic potential. He noted that a charge, whose intensity over an elliptical region on the surface of a conductor varies as the coordinate of a semi-ellipsoid, gives

rise to a variation in potential throughout that surface which is parabolic.

By analogy, the pressure distribution is given by the equation

$$p = p_0 \sqrt{1 - (x/a)^2 - (y/b)^2} \quad (2.13)$$

The pressure distribution is semi-ellipsoidal and, from the known volume of an ellipsoid, it can be concluded that the total load P is given by

$$P = 2/3 p_0 \pi a b \quad (2.14)$$

from which the average pressure

$$p = 2/3 p_0 \quad (2.15)$$

2.7.1 For line contacts (with load P per unit length)

Semi-Contact Width:

$$a = \sqrt{4 P R / \pi E'} \quad (2.16)$$

Max-Contact Pressure:

$$p_0 = 2 P / \pi a = \sqrt{(P E^* / \pi R)} \quad (2.17)$$

Max.-Shear Stress:

$$\tau_1 = 0.3 p_0 \quad \text{at } x = 0, z = 0.78 a \quad (2.18)$$

2.7.2 For circular point contacts (Load P)

Radius of Contact Circle:

$$a = (3 P R / 4 E^*)^{1/3} \quad (2.19)$$

Max. Contact Pressure:

$$p_0 = 3 P / 2 \pi a^2 = (6 P E^{*2} / \pi^3 R^2)^{1/3} \quad (2.20)$$

Approach of distant points:

$$\delta = a^3 / R = (9 P^2 / 16 R E^{*2})^{1/3} \quad (2.21)$$

Max. Shear Stress:

$$\tau_1 = 0.31 p_0 \quad \text{at } r = 0, z = 0.48 a \quad (2.22)$$

Max. Tensile Stress:

$$\sigma_r = (1-2\nu)p_0 \quad \text{at } r = a, z = 0 \quad (2.23)$$

2.7.3 For elliptical point contact (Load P)

Equivalent Radius of Curvature:

$$R_e = \sqrt{(R' R'')} \quad (2.24)$$

Max. Contact Pressure:

$$p_0 = 3 P / 2 \pi a b = (6 P E^{*2} / \pi^3 R_e^2)^{1/3} \quad (2.25)$$

Approach of Distant Points:

$$\delta = (9 P^2 / 16 R_e E^{*3})^{1/3} \quad (2.26)$$

From equation (2.21) the approach may be rewritten as

$$\delta^3 = 9 P^2 / 16 R E'^2 \quad \text{giving} \quad (2.26)$$

$$P = 4 E' R^{1/2} \delta^{3/2} / 3$$

whose differentiation with respect to δ gives radial stiffness of a circular Hertzian contact as

$$K = \frac{dP}{d\delta} = 2 E' R^{1/2} \delta^{1/2}$$

substituting for δ gives

$$K = (6 E'^2 R P)^{1/3} \quad (2.27)$$

Similarly for an elliptical contact in which

$$P = 4 (R_e^{1/2} E' \delta^{3/2})$$

and

$$K = \frac{dP}{d\delta} = 2 R_e^{1/2} E' \delta^{1/2}$$

substituting for δ gives

$$K = (6 E'^2 R_e P)^{1/3} \quad (2.28)$$

Equations 2.27 and 2.28 can be expressed as

$$K = C P^{1/3} \quad (2.29)$$

where C takes on the appropriate constant depending on whether the stiffness referred to is for a circular or elliptical contact zone. It can be seen that equation 2.29 is non-linear however, for small amplitudes it is sufficient to assume a constant radial stiffness, viz.,

$$K = \left| \frac{dP}{d\delta} \right|_{P_0} \quad (2.30)$$

where P_0 is the applied static normal load with which the contact oscillates.

2.8 Longitudinal stiffness of the contact

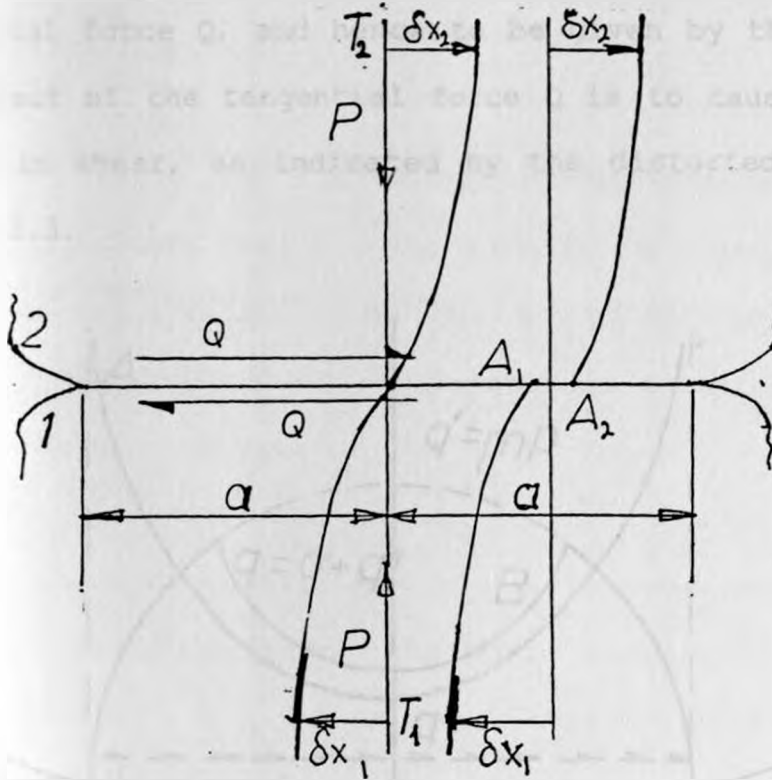


Fig.2.3 Tangential surface tractions which arise from a combination of normal and tangential forces which do not cause the bodies to slide relative to each other.

A tangential force whose magnitude is less than the force of limiting friction, when applied to two bodies pressed into contact, will not give rise to a sliding motion but nevertheless, will induce frictional tractions at the contact

interface. The problem is illustrated in Fig.2.3. The normal force P gives rise to a contact area and pressure distribution which is assumed to be influenced by the existence of the tangential force Q , and hence to be given by the Hertz theory. The effect of the tangential force Q is to cause the bodies to deform in shear, as indicated by the distorted centre-line in figure 2.3.

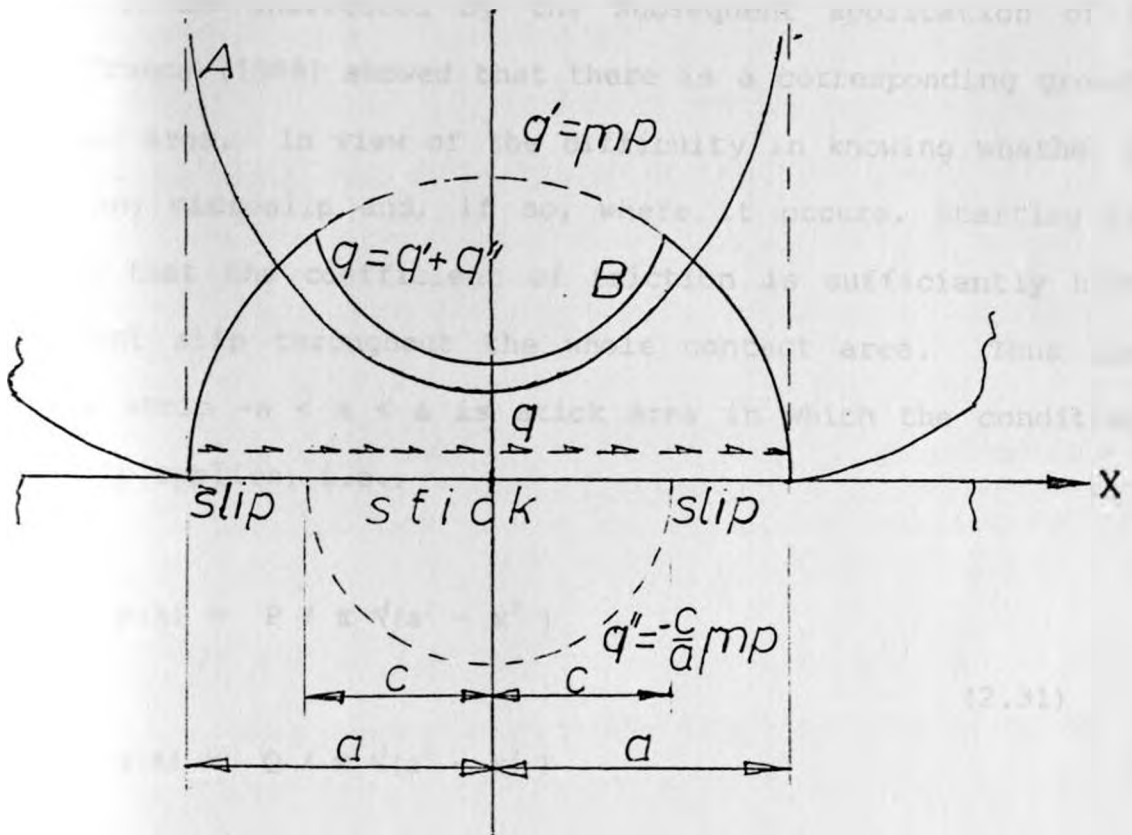


Fig.2.4 Contact of cylinders with their axes parallel. Surface tractions due to a tangential force $Q < \mu P$. Curve A- no slip, Curve B - partial slip.

Considering two cylinders in contact with their axes parallel to the y- axis, compressed by a normal force P per unit axis length to which a tangential force Q per unit length is subsequently applied. (See Fig. 2.4).

The contact width and the pressure distribution due to P are given by the Hertz theory. For simplicity these quantities are assumed to be unaffected by the subsequent application of Q though Prancs [1988] showed that there is a corresponding growth in actual area. In view of the difficulty in knowing whether Q causes any microslip and, if so, where it occurs, starting by assuming that the coefficient of friction is sufficiently high to prevent slip throughout the whole contact area. Thus the complete strip $-a < x < a$ is stick area in which the condition of no-slip applies, i.e.,

$$p(x) = P / \pi \sqrt{(a^2 - x^2)}$$

and

(2.31)

$$q(x) = Q / \pi \sqrt{(a^2 - x^2)}$$

The traction given by equation 2.31 is plotted in Fig. 2.4 (Curve A). It rises to a theoretically infinite value at the edges of the contact. The points $x = \pm a$ then appears as the tips of two sharp deep cracks in the sides of a large solid block, where singularities in stress would be expected.

If the tangential force Q is increased to its limiting value μP , so that the bodies are on the point of sliding, the tangential traction is given by

$$q'(x) = \mu p_0 \sqrt{[1 - (x/a)^2]} \quad (2.32)$$

where

$$p_0 = 2 P / \pi a \quad (\text{Line contact})$$

Consider an additional distribution of traction given by

$$q''(x) = -c \mu p \sqrt{[1 - (x/a)^2]} / a \quad (2.33)$$

acting over the strip $-c < x, < c$ ($c < a$), as shown in Fig. 2.4. Furthermore in this region the resultant traction is given by

$$\begin{aligned} q(x) &= q'(x) + q''(x) \\ &= \mu p_0 [\sqrt{(a^2 - x^2)} - \sqrt{(c^2 - a^2)}] / a \end{aligned} \quad (2.34)$$

which is everywhere less than μp . The size of the stick region is determined by the magnitude of the tangential force.

$$\begin{aligned} Q &= \int_{-a}^a q(x) dx = \int_{-a}^a q'(x) dx + \int_{-c}^c q''(x) dx \\ &= \mu P - (c/a)^2 \mu P \end{aligned}$$

so that

$$c/a = \sqrt{1-Q/\mu P} \quad (2.35)$$

The physical behaviour is now clear. If, keeping P constant, Q is increased steadily from zero, micro-slip begins immediately at the two edges of the contact area and spreads inwards according to equation 2.35. As Q approaches μP , c approaches zero and the stick region shrinks to a line at $x = 0$. Any attempt to increase Q in excess of μP causes the bodies to slide.

According to Deresiewicz [1957], the tangential stiffness for a toroid- cylinder contact is given by

$$K_t = 8 a G_1 G_2 (1 - Q/\mu P)^{1/3} / [G_1(2-\nu_1) + G_2(2-\nu_2)] \quad (2.36)$$

Fig. 2.5 gives the plot of the ratio of the tangential stiffness to the maximum possible value against the traction load ratio. It can be seen that the contact would lose its tangential stiffness when full sliding occurs with the tangential force $Q = \mu P$.

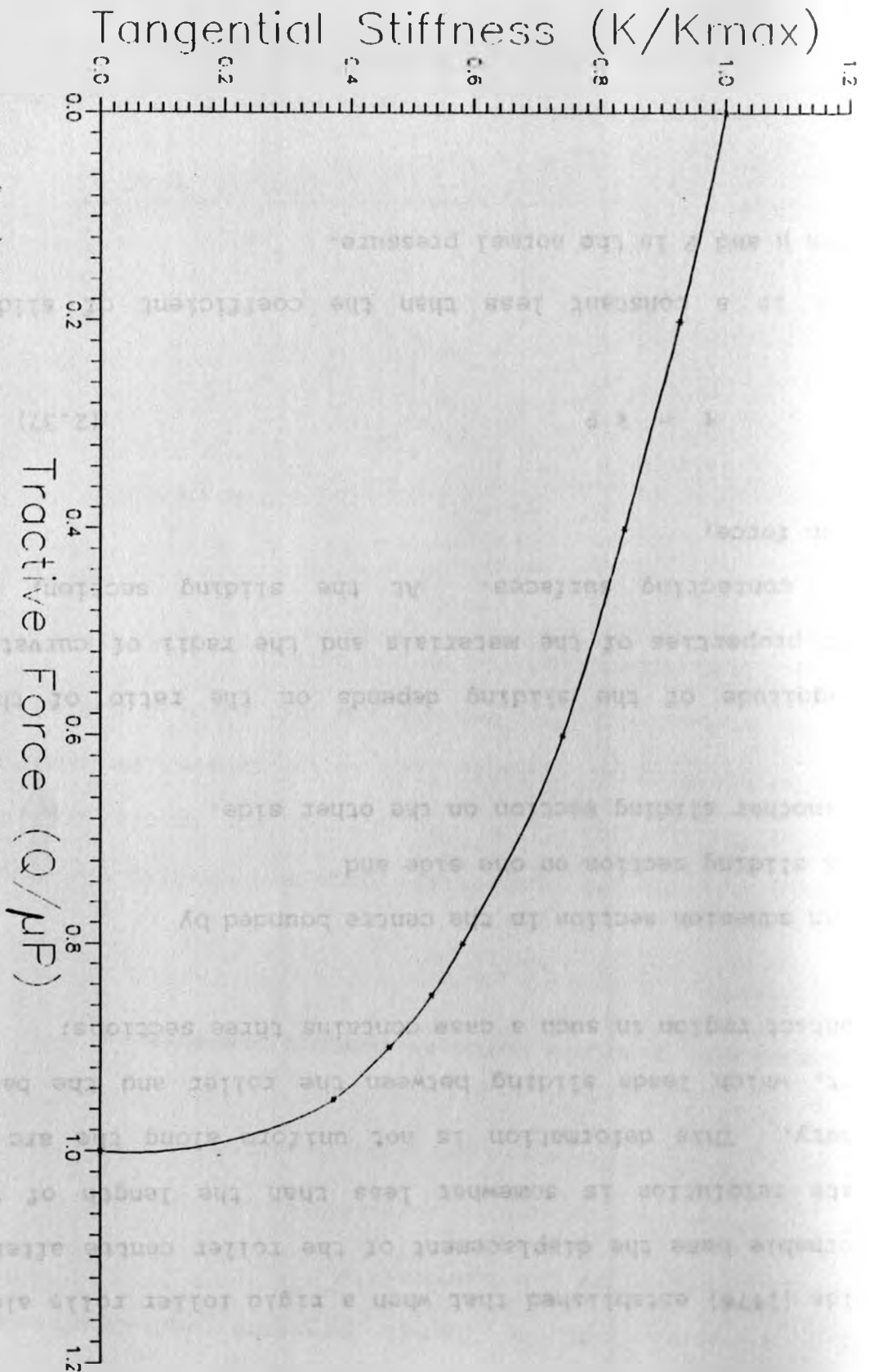


Fig. (2.5) Curve of variation of Tangential Stiffness with tractive force

2.9 Sliding as one of the sources of resistance to rolling

Reynolds [1876] established that when a rigid roller rolls along a deformable base the displacement of the roller centre after a complete revolution is somewhat less than the length of the periphery. This deformation is not uniform along the arc of contact, which leads sliding between the roller and the base. The contact region in such a case contains three sections;

- i) an adhesion section in the centre bounded by
- ii) a sliding section on one side and
- iii) another sliding section on the other side.

The magnitude of the sliding depends on the ratio of the elastic properties of the materials and the radii of curvature of the contacting surfaces. At the sliding section, the friction force,

$$\tau = k P \quad (2.37)$$

where k is a constant less than the coefficient of sliding friction μ and P is the normal pressure.

At the adhesion section, the velocities of the points on the surfaces are equal and the normal pressure and frictional stresses are connected by the inequality

$$\tau < \mu P \quad (2.38)$$

2.10 The effect of tractive force on contact pressure distribution

In railroads, substantial tangential loads are created by wheel braking, and the lateral loads are created by impure rolling action. The presence of a tangential force causes the maximum value of the contact stresses between the two elastic bodies to become larger than those produced by the normal force.

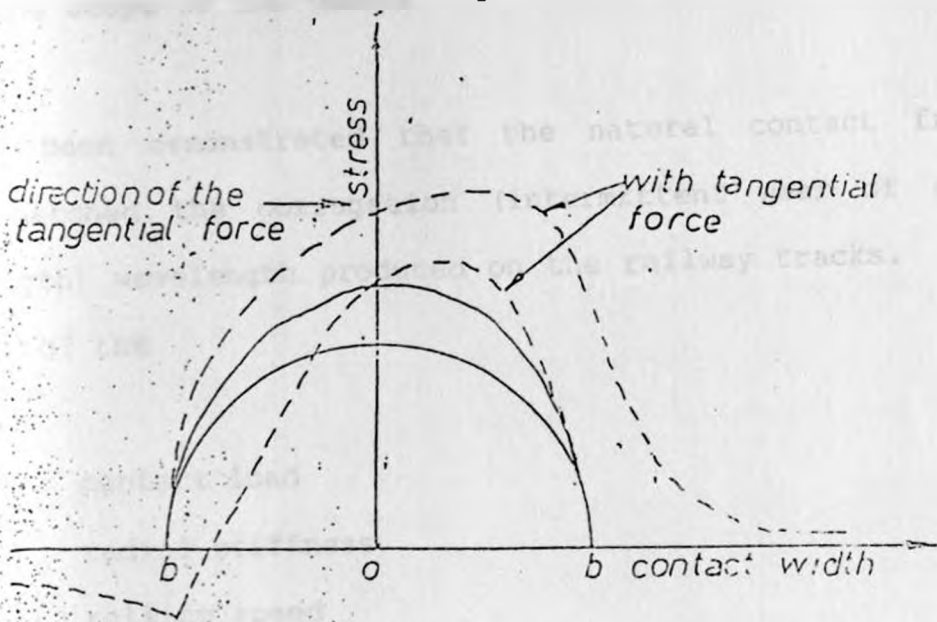


Fig. 2.6 Schematic diagram of principal stresses of surfaces of cylinders loaded both radially and tangentially.

The dashed curves in figure 2.6 show the relationship between the tangential loads and the principal stresses for the case of a wheel on rail. It has been shown that the normal stress with a tangential load one-third the radial load reaches 1.4 times that resulting from radial loading alone, Meacham [1964]. Although the magnitude of the maximum shear stress still retains a value of about one-third the maximum normal stress, the location of the maximum shear stress changes from beneath the surface of contact for tangential loads exceeding 0.1 of their radial loads. In addition, there is a tensile stress at the leading edge of the contact area, which changes the cyclic stress pattern from a released-type loading to a more severe reversed-type loading.

2.11 The scope of the thesis

It had been demonstrated that the natural contact frequency often matched the corrugation (intermittent wear of constant wavelength) wavelength produced on the railway tracks. But the effects of the

- i) contact load
- ii) radial stiffness
- iii) rolling speed
- iv) lateral movement and

v) tractive force

on the formation of corrugation and its wavelength had not quantitatively been established. This was the area investigated in the study. Mathematical models of a rolling system was developed from which the response of the system to the above parameters computed and finally experiments were done on a rolling rig and the theoretical predictions and the experimental results compared.



CHAPTER THREE

3. EXPERIMENTAL APPARATUS

3.1 The rolling rig

The dynamic system chosen for study of dynamics of contact surfaces under pure rolling and rolling with traction conditions comprises a pair of discs coupled by the elastic contact formed as a result of the elastic loading of the discs which acts as a spring as illustrated in figure 3.1.

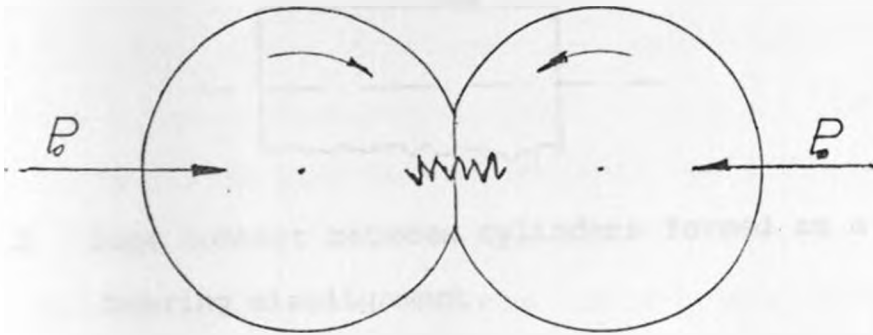


Fig. 3.1 Dynamics of a rolling contact system.

This system must be assembled in such a way that the supports do not influence the fundamental mode of vibration of the discs, that is by bearings and shafts whose stiffness are not comparable to that of the contact.

3.1.1 Contact geometry

Production of a Hertzian contact between the surfaces of two non-conforming bodies could start as a line or point contact before the surfaces are loaded. The line contact between parallel cylinders has the main advantage in the ease with which cylinders can be machined. However, they pose an alignment problem, if edge contact is to be avoided.

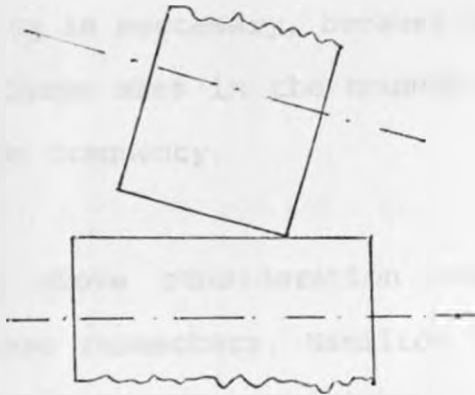


Fig. 3.2 Edge contact between cylinders formed as a result of bearing misalignment.

The edge loading problem is overcome by the use of a deforming crowned disc hardened and tempered to VHN 800 with disposable cylindrical test pieces. This toroid-cylinder combination permits one to consume cylinders rather than toroids, with a considerable saving of machining time. The toroid was manufactured by turning on a C.N.C. machine and its views are as shown in figure 3.3.

It should be noted that according to Carson [1970] self alignment of the combination is only possible if the crown radius of the toroid is equal to or greater than the rolling radius.

3.1.2 Upper arm size

The upper-arm size has a significant influence on the contact frequency. A large pivoted arm of size 165mm by 130 mm by 60 mm and weighing 12 Kg is necessary, because it permits the designer to concentrate a large mass in the housed roller, thereby lowering the its vibration frequency.

Because of the above consideration and bearing in mind the experience of past reseachers, Hamilton [1963], the optimum size for both the toroid and the cylindrical test piece was taken to be 100 mm diameter (to allow measurable corrugation wavelengths to form) with an effective width of 20 mm (for adequate contact stresses to be produced by moderate loads) housed in a box-like case as shown in figure 3.7.

3.1.3 Bearing type

Rolling contact bearings are excluded because of the variation of stiffness with the passage of each roller which introduces a normal excitation. Plain journal bearings, even though having the problem of varying stiffness with speed, were adopted. This was because they were easy to construct and could be adequately lubricated using grease.

3.1.4 Wear and corrugation test materials

Between tests any pick up of soft material on the hard disc was lapped off in situ by pressing an abrasive paper against the rolling disc, this of course did not disturb the crown geometry which is critical in determining the contact dynamics.

The disposable discs were made from aluminium, perspex and mild steel. To avoid damaging the hard disc rolling tests were done first on the softer perspex then followed by aluminium, and mild steel in that order.

3.2 Contact frequency

The radial contact frequency must not be too high for two reasons:

- i) A high contact frequency demands the running of the rig at high peripheral velocity to ensure that the surface of the test piece is intermittently worn.
- ii) It becomes increasingly difficult to measure mechanical vibrations at frequencies in excess of about 1.5 KHz (experimentally determined), because spurious resonances of the machine structure will interfere.

The design therefore aimed at a contact frequency less than 1.0 KHz which is fixed by the contact stiffness and the effective mass resting on the lower disc. For design contact stiffness of about 400 MN/m and an effective upper-arm mass of 12 Kg the contact frequency would be

$$\begin{aligned} f_n &= 0.5 \pi (K/m)^{1/2} && (3.1) \\ &= 919 \text{ Hz.} \end{aligned}$$

This frequency value is well above the structure resonance (as calculated from the values of the loading spring stiffness and the vibrating mass) brought about by the loading spring and its effects could be easily isolated.

3.3 The contact load

For the elastic loading of the rollers p_0/k ratio must not exceed 3, where p_0 is the maximum Hertzian compressive stress and k the shear flow stress of the softer material, Johnson [1962]. The maximum contact pressure for an extreme case of a line contact is given by equation 2.16.

$$p_0 = 2 P / \pi a = (P E^* / \pi R)^{1/2}$$

giving the critical load per unit length as

$$P = 9 \pi R k^2 / E^* \quad (3.2)$$

For steel/steel pair of rollers of diameter 100 mm and width 20 mm we have

$$\begin{aligned} E^* &= \left\{ (1-\nu_1^2)/E_1 + (1-\nu_2^2)/E_2 \right\}^{-1} \\ &= 1.0989 * 10^{11} \text{ N m}^{-1} \end{aligned}$$

giving

$$P = 123,602 \text{ N.}$$

The maximum load the rig should transmit to 20 mm thick discs is a fiftieth that on a metre length, that is about 2,500 N which became the design load for the rig parts.

3.4 The loading spring

Because the loading arm had an effort magnification of about two the loading compression spring was designed to transmit half the maximum load required for the plastic deformation of steel test pieces, i.e., able to exert at least 1,250 N when fully compressed. A standard coil spring chosen had the following characteristics:

Modulus of rigidity	$G = 80 \text{ GPa.}$
Coil diameter	$D = 25 \text{ mm.}$
Wire diameter	$d = 4 \text{ mm.}$
Number of coils (effective)	$n = 8$

It had a stiffness given by

$$K = \frac{G d^4}{8 D^3 n} \quad (3.3)$$

$$= 20,480 \text{ N/m}$$

i.e., the stiffness of the loading spring was about 2 Kg/mm and was required to produce maximum compression at a deflection of

$$\delta = 1,250\text{N}/20,280 \text{ N/m} = 0.061 \text{ m} = 61 \text{ mm}$$

for a square ground ended coil spring:

$$\text{Solid height} = (n+2) d = 10 * 4 = 40 \text{ mm}$$

allowing 20% working compression to prevent closing of the coils during operation gave

$$\text{Max. compression} = 1.2 * 61 = 73.2 \text{ mm}$$

and hence the free length of the spring was

$$l = 73.2 + 40 = 113.2 \text{ mm}$$

the pitch was then

$$\text{pitch} = (l-2d)/n = 13.15 \text{ mm.}$$

3.5 Forced excitation of the stationary discs and response recording units

Forced excitation and response recording units facilitate the location of peak or excessive vibration frequencies of the rigs active member so that the mode frequencies responsible for corrugation formation can be experimentally identified. The units were also invaluable at all stages of design and production testing, where the detrimental effects of noisy operation had to be avoided.

The frequency range is covered in three bands, e.g.,

10	-	100	Hz	*	1
100	-	1,000	Hz	*	10
1,000	-	10,000	Hz	*	100

the reading being multiplied by the appropriate factor as indicated on the frequency multiplication switch. In our experiments the middle range of frequency (100 - 1,000 Hz) was adequate for the systems resonance within the loading limit on the roller contacts.

The frequency was controlled by the knob coupled to the frequency dial which is a slow motion drive to enable fine tuning of the oscillator frequency.

The amplitude of the oscillations is controlled by the output control knob which adjusts a potentiometer to vary the oscillator driving signals to the exciter amplifier. This effectively controls the output of the amplifier, or in other words, the current fed to the vibration generator.

The vibration detection unit comprises a vibration pickup, a cathode follower probe and the main electronic unit incorporating a high gain amplifier, intergrating and differentiating networks, an adjustable attenuator and a direct reading indicating millivoltmeter.

The vibration pickup, which is an accelerometer type, gives an output voltage proportional to the acceleration of the motion of the pivoted arm end onto which it is screwed. This pickup could operate over frequency range 1.6 to 10,000 Hz and has sensitivity high enough for application in this particular set up. The voltage from the accelerometer is fed into the input of the high impedance probe. The probe incorporates a subminiature valve and a transistor in a cathode follower circuit, to obtain very high input impedance and low output impedance. The required high tension and low tension supplies for the cathode follower are obtained from a

transistor converted circuit built into the probe unit and transistor taking supply off the battery in the main electronic circuit.

The signal voltage from the cathode follower probe is taken to the main electronic unit and in the case of acceleration directly through an adjustable attenuator to the first two stages of the amplifier. The amplified signal is fed through another attenuator and the last two stages of the amplifier, where it is used to drive an indicating meter calibrated in absolute vibration units in millivolts. The meter circuit is made to respond to either positive or negative peak, full-wave average or quasi-r.m.s. values of the applied vibration waveform.

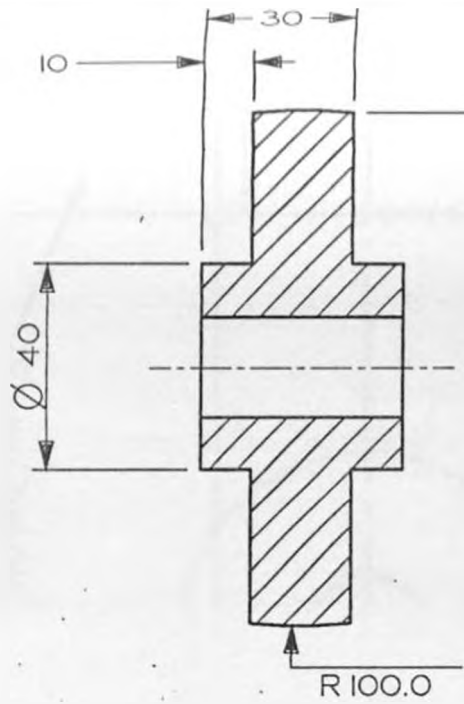
3.6 The motor drive unit

The drive unit for the corrugation rig consisted of an electric motor and an infinite speed ratio gearbox coupled to the driving shaft of the machine. The coupling which connected the output shaft of the gearbox and the rigs driving shaft was designed to adequately transmit the rolling torque while reducing the transmission of shock loads from the driving motor to the rolling

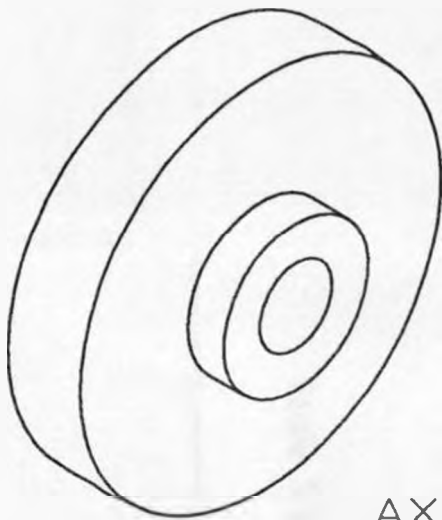
surfaces. It could also take any misalignment of the shafts thereby bringing in mechanical flexibility. The protection against the overload of the machine is taken care of by the cotter pin fixing the coupling to the rigs driving shaft.

Once the drive from the motor reaches the driving shaft onto which the test disc is fixed the crowned disc then is rotated through friction as it is radially loaded to the other disc. Braking force is applied through the traction belt to the driven disc whose speed is reduced relative to that of the driving disc as a consequence of belt friction.

67



SECTION XX



AXONOMETRIC

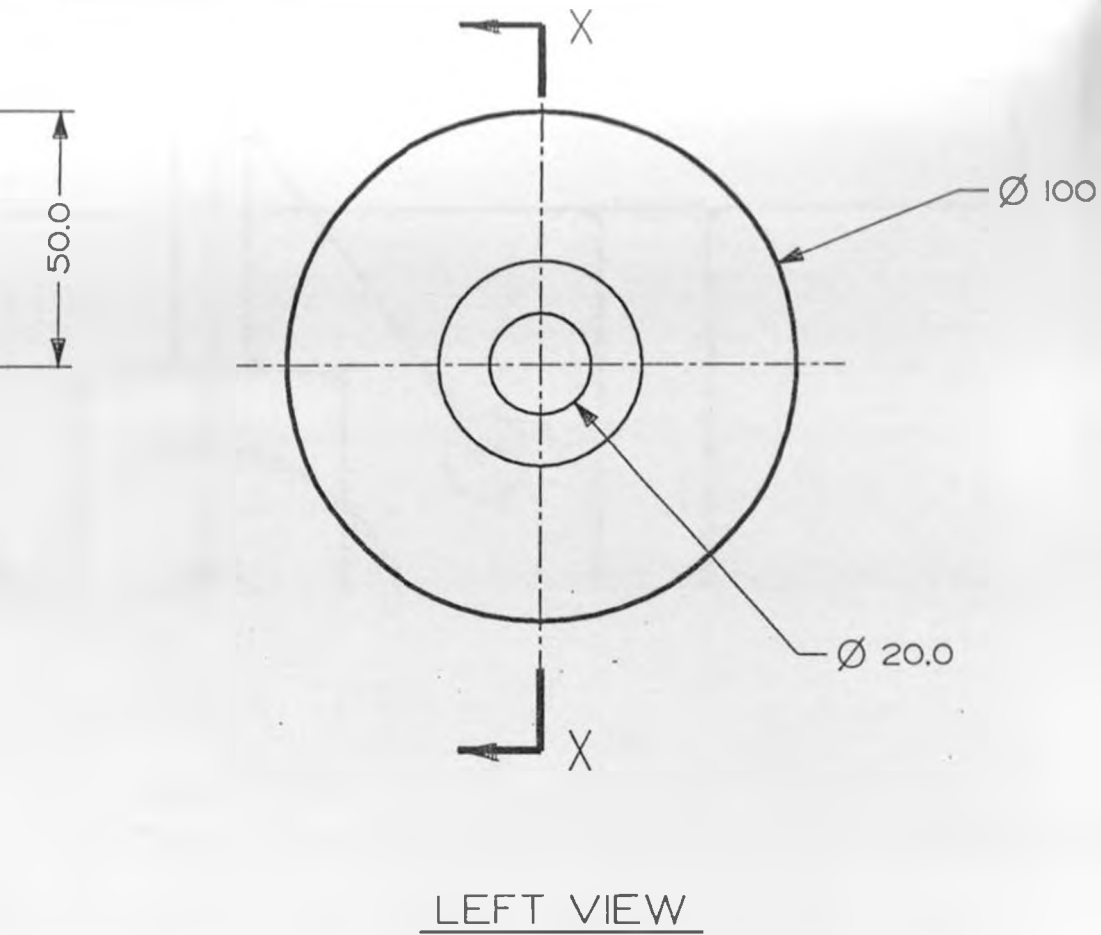


Fig. 3.3 Views of the toroid

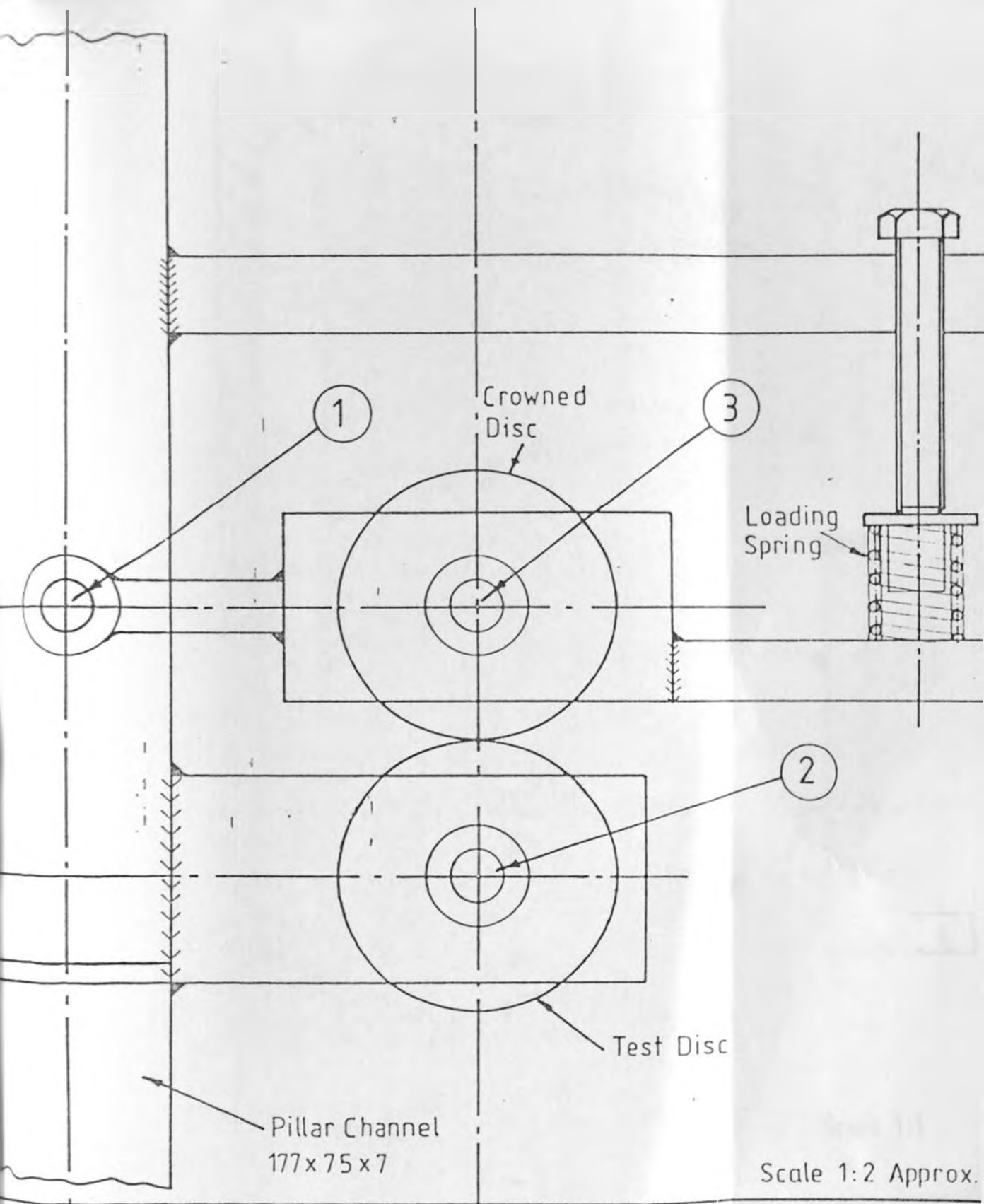


Fig. (3.4) Front View of the Rolling Rig Showing the Main Assemblies 1, 2 and 3. detailed in Fig. 3.5 to 3.7.

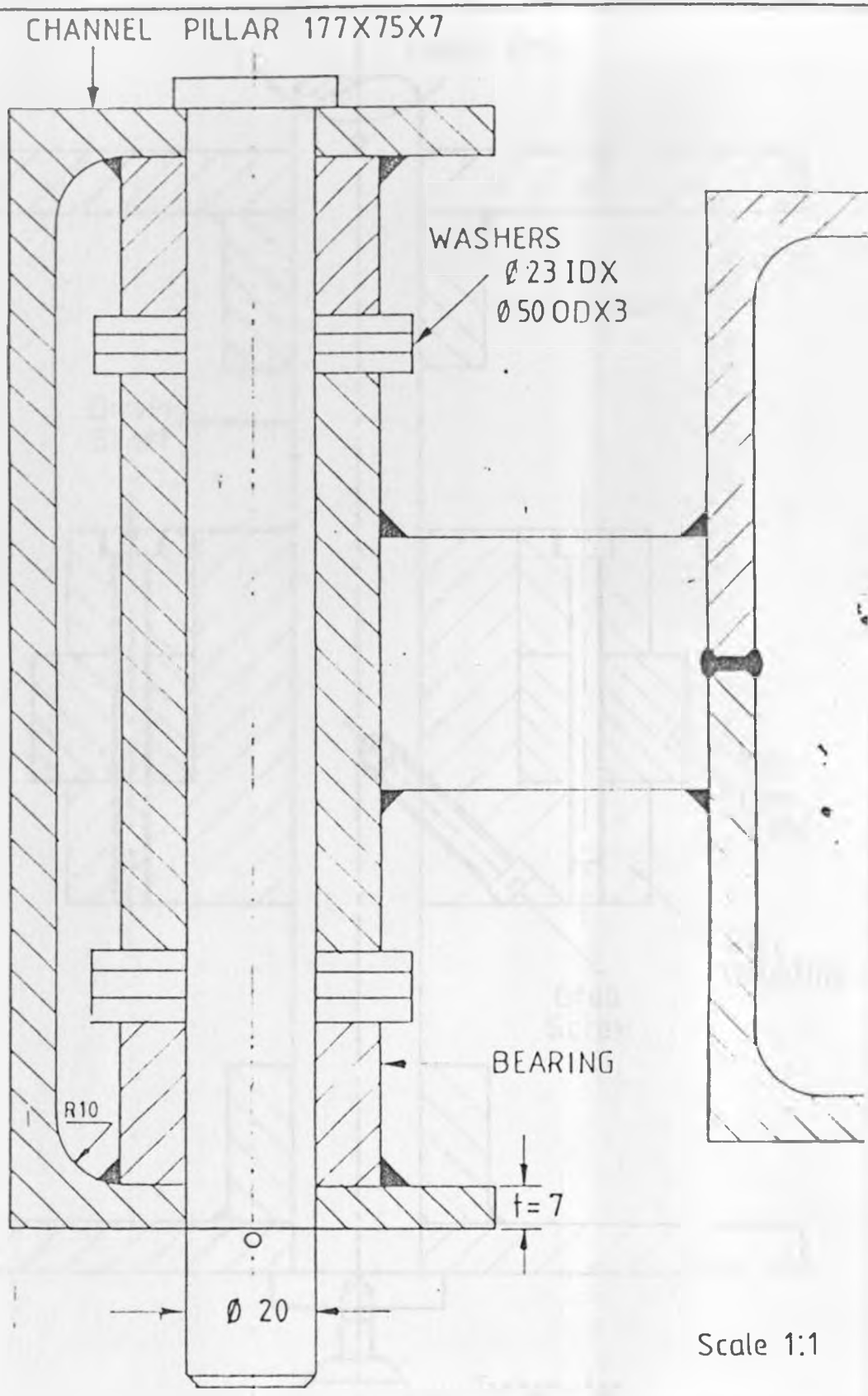
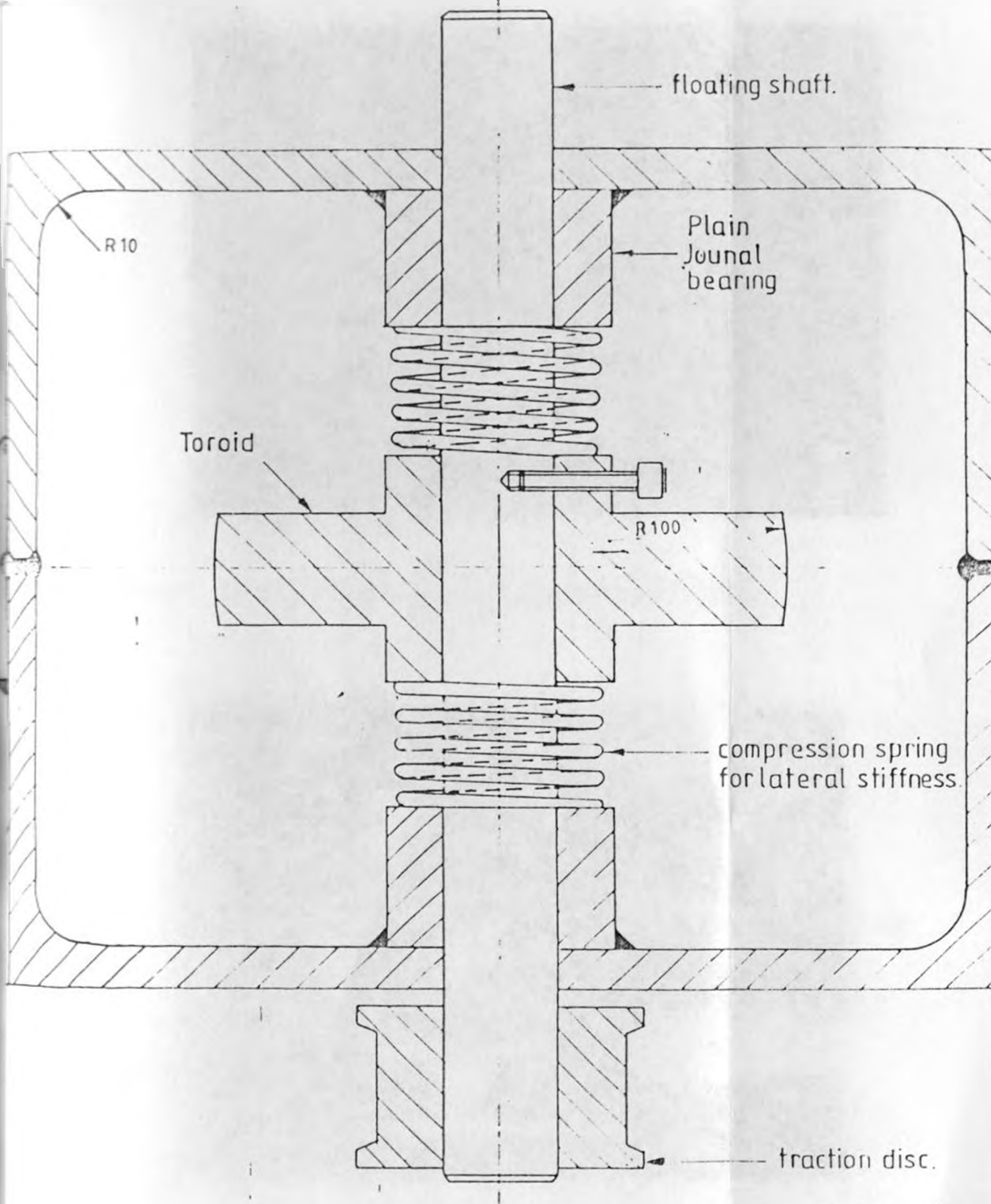


Fig. [3-5] Pivot Assembly (1)



scale 1:1

[37] Crowned Disc Housing Assembly

3



PLATE (3.1) THE MOTOR AND GEAR BOX ASSEMBLY.



PLATE (3.2) THE PIVOTED ARM ASSEMBLY.

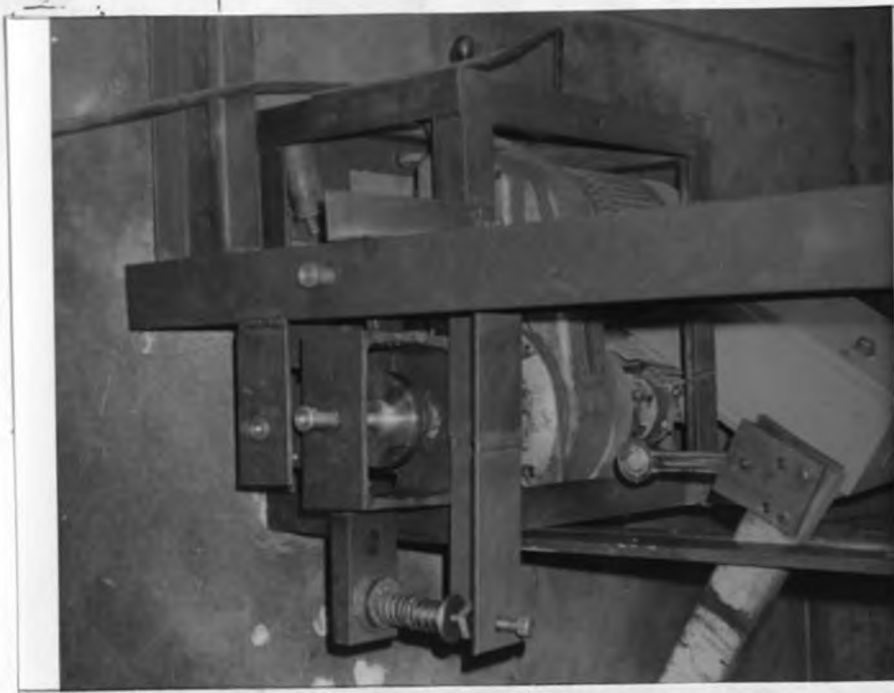


PLATE (.3.3) THE ROLLING RIG MACHINE.



PLATE (3.4) THE TEST DISC HOLDER.



PLATE (3.5) SOME OF THE CORRUGATED TEST DISCS.

CHAPTER FOUR

4. EXPERIMENTAL PROCEDURE

4.1 Calibration of the loading bolt turns

The amount of the load on the discs can be obtained by employing the use of foil resistance strain gauges fixed on the strained part of one of the members. However, it was observed that the loading spring deflection, measured by a dial gauge, was an accurate and reliable indication of the load transmitted to the discs, and this method was adopted for the radial loading of the discs.

Theoretically the axial stiffness of a square ended coil spring is given by the expression

$$K_s = \frac{G d^4}{64 R^3 n} \quad (4.1)$$

where

G is the modulus of rigidity of the spring material

d is the spring wire diameter
 R is the radius of the coil and
 n is the number of active turns of the coil.

For the loading spring in question, $G = 80 \text{ G Pa}$, $d = 4 \text{ mm}$, $R = 12.7 \text{ mm}$, and $n = 14$ complete turns. It therefore has

$$K_s = \frac{80 * 10^9 * 0.004^4}{64 * 0.0127^3 * 8} = 19,257.6 \text{ N/m}$$

Using dead weights to provide the compressing force and employing the deflection of a dial gauge pointer to measure the coil compressions the axial stiffness of the spring was experimentally determined.

4.2 Determination of the approach of distant points with radial contact force for various roller material combinations

By loading the discs as shown in figure 4.1 the apparent approaches for the corresponding contact forces were determined using the dial gauge indicator to measure the approach. It is expected that initial loading of the discs produced relatively large approaches

of distant points on the two bodies. This could be due to the contact which is initially a point hence can not support a large force and therefore deforms rapidly due to the high stresses initially created. With further increase in the load the surface area increases proportionately and that accounts for the steady increase of the approach with the load in the subsequent loading till the plastic yielding load. Beyond the yield load creep increases the approach without any appreciable increase of the contact force. For the experimental results the radial contact load P is given Newtons while the approach of distant points δ is in μm .

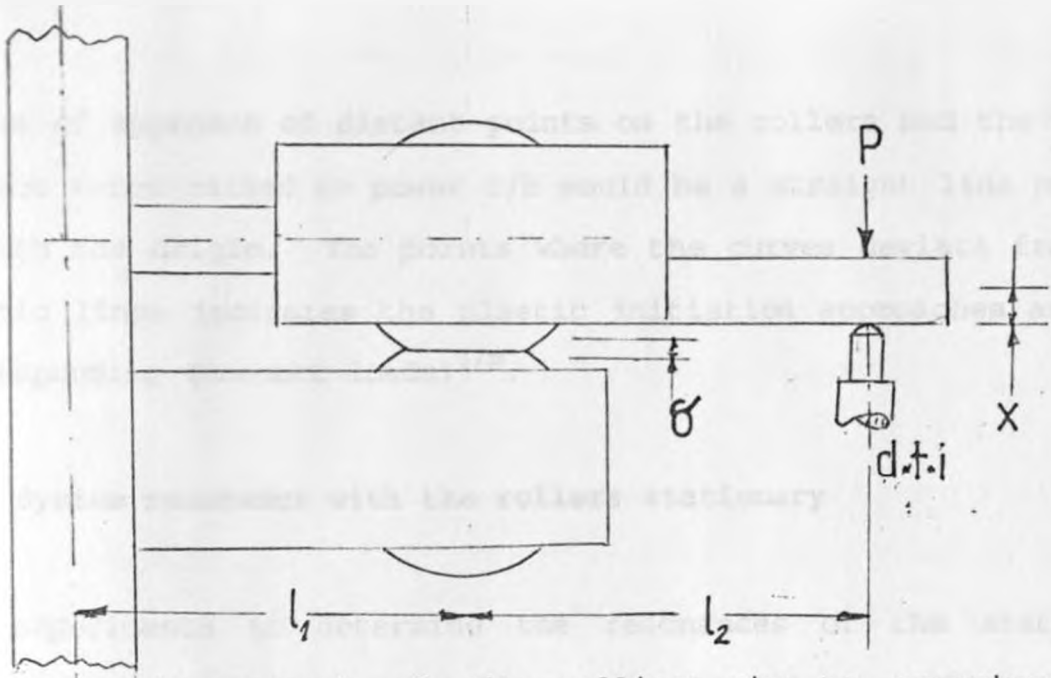


Fig. 4.1 Arrangement of the rolling rig to experimentally determine the approach of distance points on the rollers with the radial contact force.

4.3 Plastic initiation contact forces

The general contact load-approach relationship for the elastic deformation of the contact zone for non-conforming bodies can be written as

$$\delta = C^* P^{1/b} \quad (4.2)$$

where $C^* = C^{-1/b}$

A plot of approach of distant points on the rollers and the radial contact force raised to power $1/b$ would be a straight line passing through the origin. The points where the curves deviate from the elastic lines indicates the plastic initiation approaches and the corresponding (contact loads) ^{$1/b$} .

4.4 System resonance with the rollers stationary

The experiments to determine the resonances of the stationary rollers were done when the rollers were loaded at various contact forces giving rise to different system frequencies. A shaker controlled to give vibrations in the range of 0 - 4 KHz and linked to the lower shaft excited the system from the lower roller and the response of the system was detected by a transducer screwed into the pivoted arm. From the transducer the picked up signal was directed to the filter tube which at the same time acted as amplifier. The output whose magnitude was proportional to the voltage from the filter/amplifier tube was registered as a deflection of the milliammeter pointer. The milliammeter range could be selected to suit the output magnitude which in this case was between 0 mA and 10 mA.

The excitation amplitudes were made relatively small to avoid contact stiffness non-linearity, i.e., the displacement of the contact was made to be less than the static radial approach so that bouncing of the discs could be avoided.

4.5 The rolling tests

The rolling tests were carried out when the rollers were rotated at a specified constant speed by an electric motor coupled to the lower shaft on to which the test roller was fixed. The experiments to determine the connection between the corrugation wavelength and the pure rolling speed were done on three different test disc materials loaded within the dynamic range so that good formation of corrugation could be obtained.

Those ones to show the relationship between the wear on a rolling surface of a body and the lateral movement of the contact were performed on a number of aluminium discs loaded at 500 N and rolled at 400 r.p.m. which are within the dynamic loading range and above the critical speed respectively. The lateral stiffness was altered by floating the crowned discs' shaft between two compression springs which could be changed to provide different lateral stiffnesses.

In determining the effects of the tractive force on the wear on the rolling surfaces a tractive force was applied on the driven disc so as to lower its speed relative to that of the test disc. The difference in speed of the two discs results in peripheral surface slip as given by the equation

$$\zeta = \frac{2 (N_1 + N_2)}{(N_1 + N_2)} \quad (4.3)$$

where N_1 and N_2 are the rotational speeds of the discs of equal diameter.

And finally the profiles of the corrugated surfaces were analysed from the graphs drawn on a surface profiling machine, "Tallysuf". These graphs show the profiles of the surfaces along the periphery of the discs. The graphs were plotted with a vertical exaggeration, i.e., the magnification in the vertical direction was higher than that in the horizontal direction for each plot.

CHAPTER FIVE

5. RESULTS

Table 5.1 Loading spring compressions with load and computations for the calculation of the axial stiffness.

Compressions	Load	xy	x ²
x (mm)	y (Kg)	(Kg.mm)	(mm)
1.20	2.5	3.000	1.4400
2.40	5.0	12.000	5.7600
3.55	7.5	26.625	12.6025
4.80	10.0	48.000	23.0400
6.10	12.5	76.250	37.2100
7.30	15.0	109.500	53.2900
8.50	17.5	148.750	72.2500
9.70	20.0	194.000	94.0900
10.90	22.5	245.250	118.8100
12.00	25.0	300.000	144.0000
13.10	27.5	360.250	171.6100
14.30	30.0	429.000	204.4900
15.60	32.5	507.000	243.3600
16.70	35.0	584.500	278.8900
$\Sigma x=126.15$	$\Sigma y=262.5$	$\Sigma xy=3044.125$	$\Sigma x^2=1460.8425$

Table 5.2 Experimental and theoretical plastic initiation loads for various 20 mm thick roller material test pieces.

ROLLER MATERIAL	PLASTIC INITIATION LOAD (N)		p_0/k RATIO
	THEORETICAL	EXPERIMENTAL	
Aluminium	1,312	1,400	1.774
Steel	823	900	1.811
Perspex	227	260	1.853

Table 5.3 Response of a forced excitation of the loaded contacts.

EXCITATION	R E S P O N S E (mA)		
FREQUENCY (Hz)	Perspex (250 N)	Steel (500 N)	Alum. (750)

0	0.0	0.0	0.0
200	3.7	0.5	2.3
300	2.0	1.5	1.5
500	1.2	1.2	2.2
800	5.0	3.5	4.7
1000	3.7	3.0	4.3
1500	4.0	3.0	4.6
2000	5.4	4.0	5.2
2500	7.3	6.0	6.3
2600	8.0	6.2	6.5
2800	7.5	7.2	8.4
2900	7.8	8.8	8.0
3000	8.0	8.8	8.0
3500	8.5	9.5	7.8
4000	9.4	10.2	8.0
1 peak	200 Hz - (3.7mA)	300 Hz - (1.2mA)	-----
2 peak	800 Hz - (5.0mA)	800 Hz - (3.5.A)	800 Hz - (4.7mA)
3 peak	2600 Hz - (8.0mA)	2900 Hz - (8.8mA)	2800 Hz - (8.4mA)

Table 5.4 Experimental and theoretical corrugation wavelengths for selected roller test pieces loaded at 700 N and pure rolled at various speeds.

TEST ROLLER	ROLLING SPEED (r.p.m.)	CORRUGATION WAVELENGTH (mm)	
		Experimental	Theoretical
AL1	400	2.5	2.1
AL2	350	2.1	1.8
ST2	300	1.3	1.6

Table 5.5 The dynamic load limits for various discs when purely rolled and when rolled with a tractive force (a third of the normal force)

TEST DISC MATERIAL	DYNAMIC CORRUGATION CONTACT LOAD LIMIT (N)	
	Pure rolling	Rolling with a tractive Force
Aluminium	400 - 950	300 - 700
Steel	300 - 650	200 - 500
Perspex	450 - ----	300 - ----

Table 5.6 Expected wavelengths on rollers rolled at 400 r.p.m. under different contact loads.

CONTACT LOAD P (N)	EXPECTED WAVELENGTH λ (mm)
450	2.160
500	2.152
550	2.145
600	2.139
650	2.133
700	2.128
750	2.123
800	2.118

Table 5.7 Summary of the observations made on the surfaces of aluminium test discs when free rolling of the discs was prevented by the application of a braking force to the crowned disc.

TEST ROLLER N_1 (R.P.M.)	CROWNED ROLLER SPEED N_2 (R.P.M.)	% SLIP ζ	OBSERVATIONS
400	400	0.0	corrugations $\lambda = 2\text{mm}$
400	380	5.1	good corrug. $\lambda = 2.1\text{mm}$
400	360	10.5	corrugations flattened
400	300	28.6	uniform wear
400	250	46.2	severe uniform wear

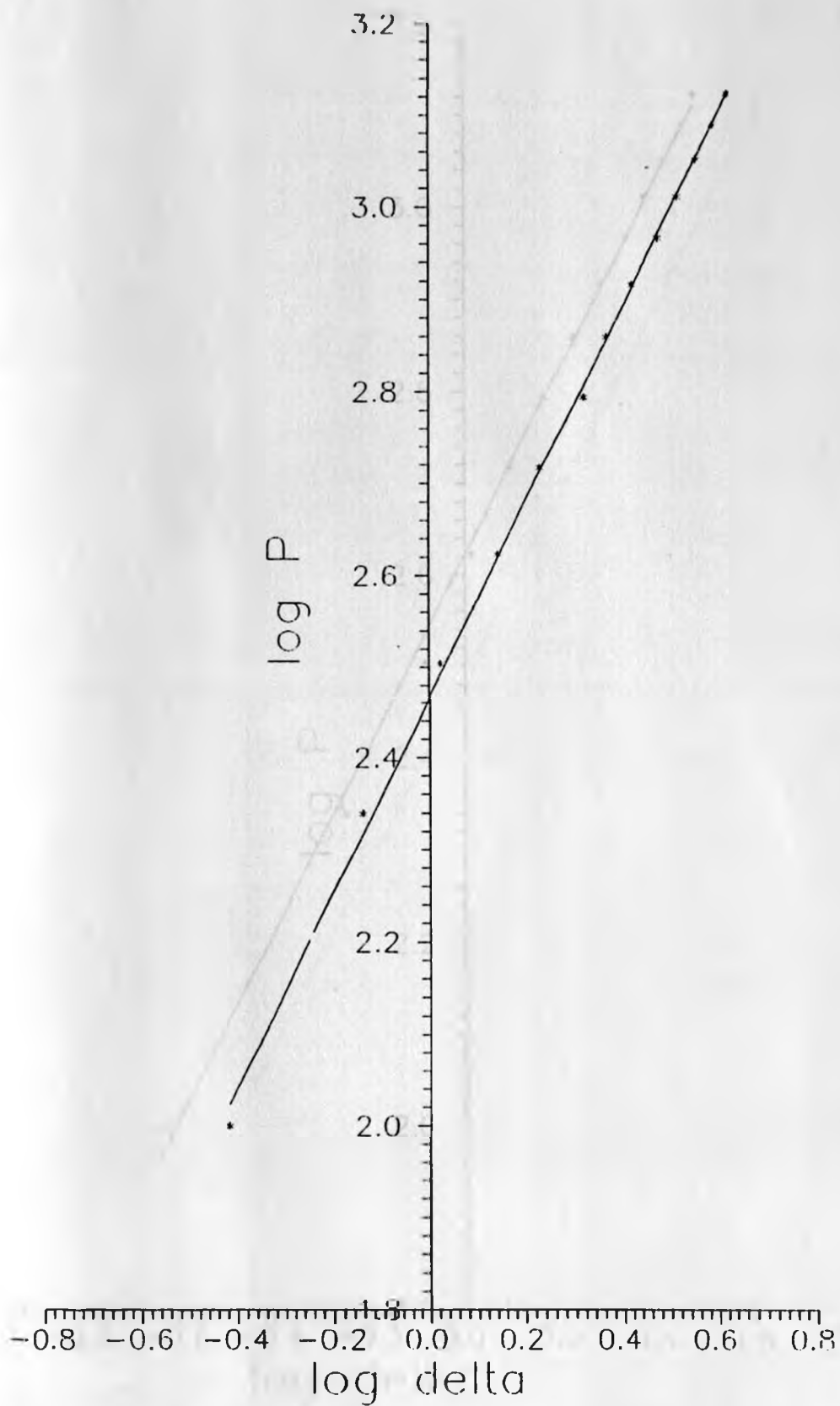


Fig. (5.1)(a) Plot of $\log P$ against $\log \delta$ for perspex test roller.

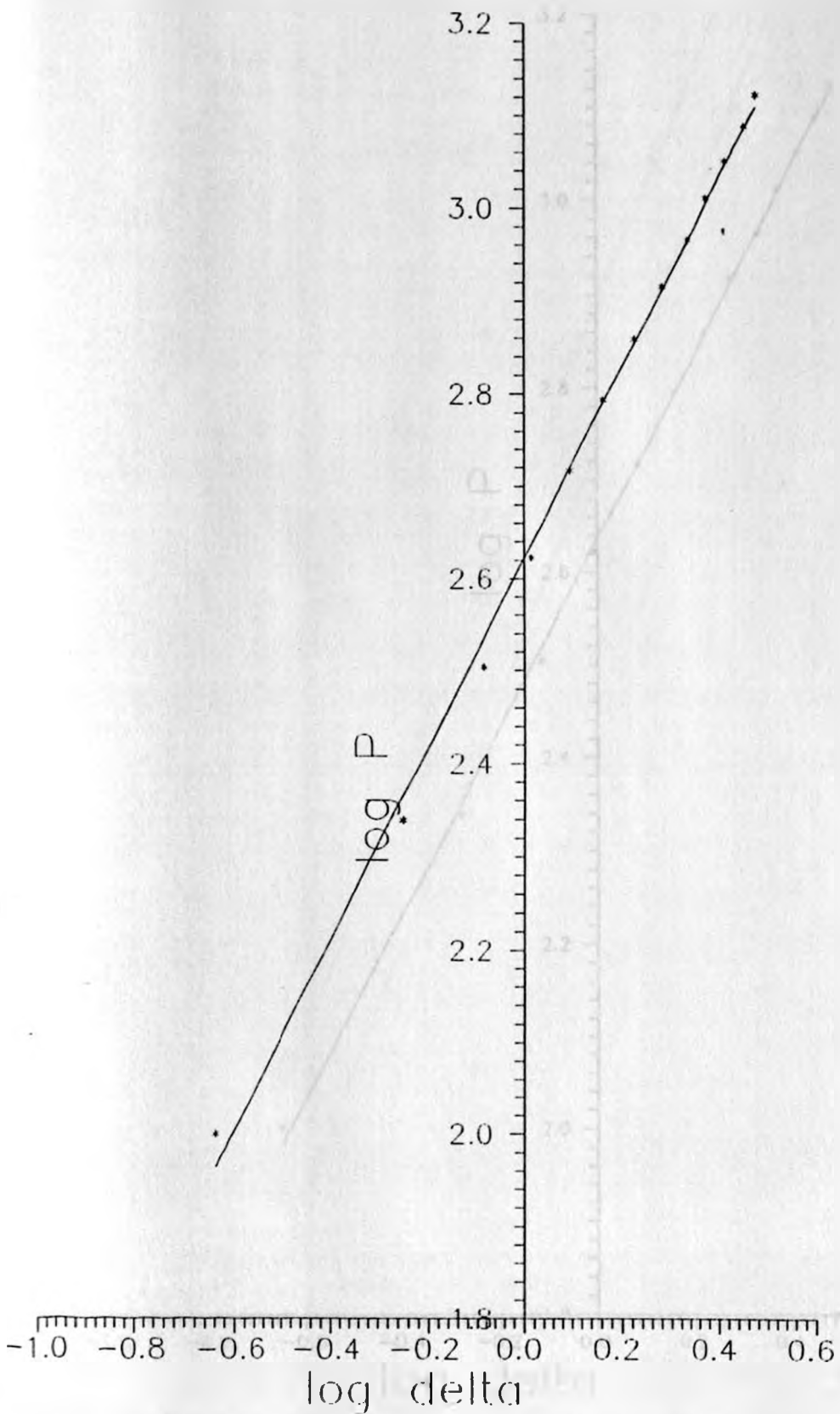


Fig. (5.1)(b) Plot of $\log P$ against $\log \delta$ for steel test roller

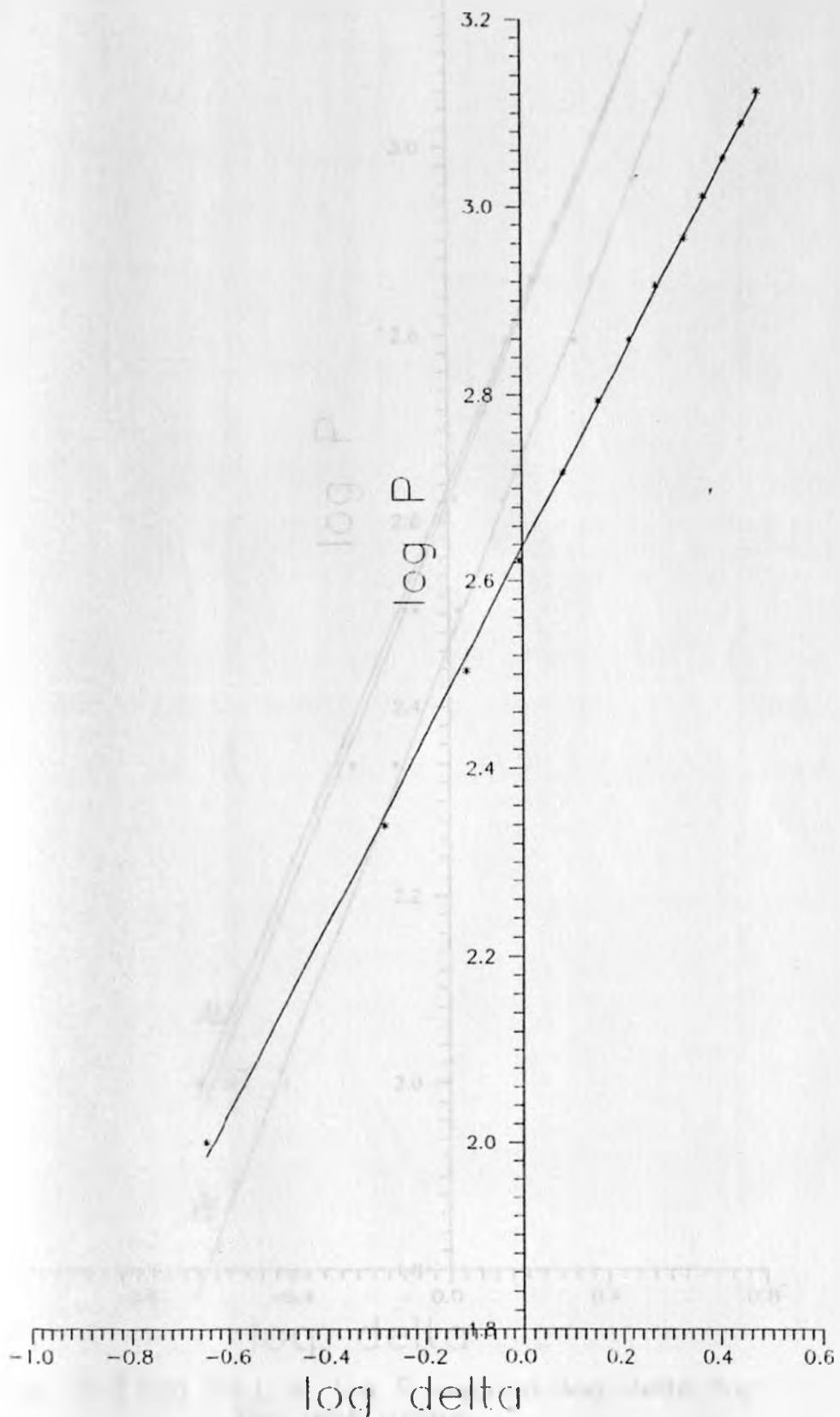


Fig. (5.1)(c) Plot of $\log P$ against $\log \delta$ for perspex test roller

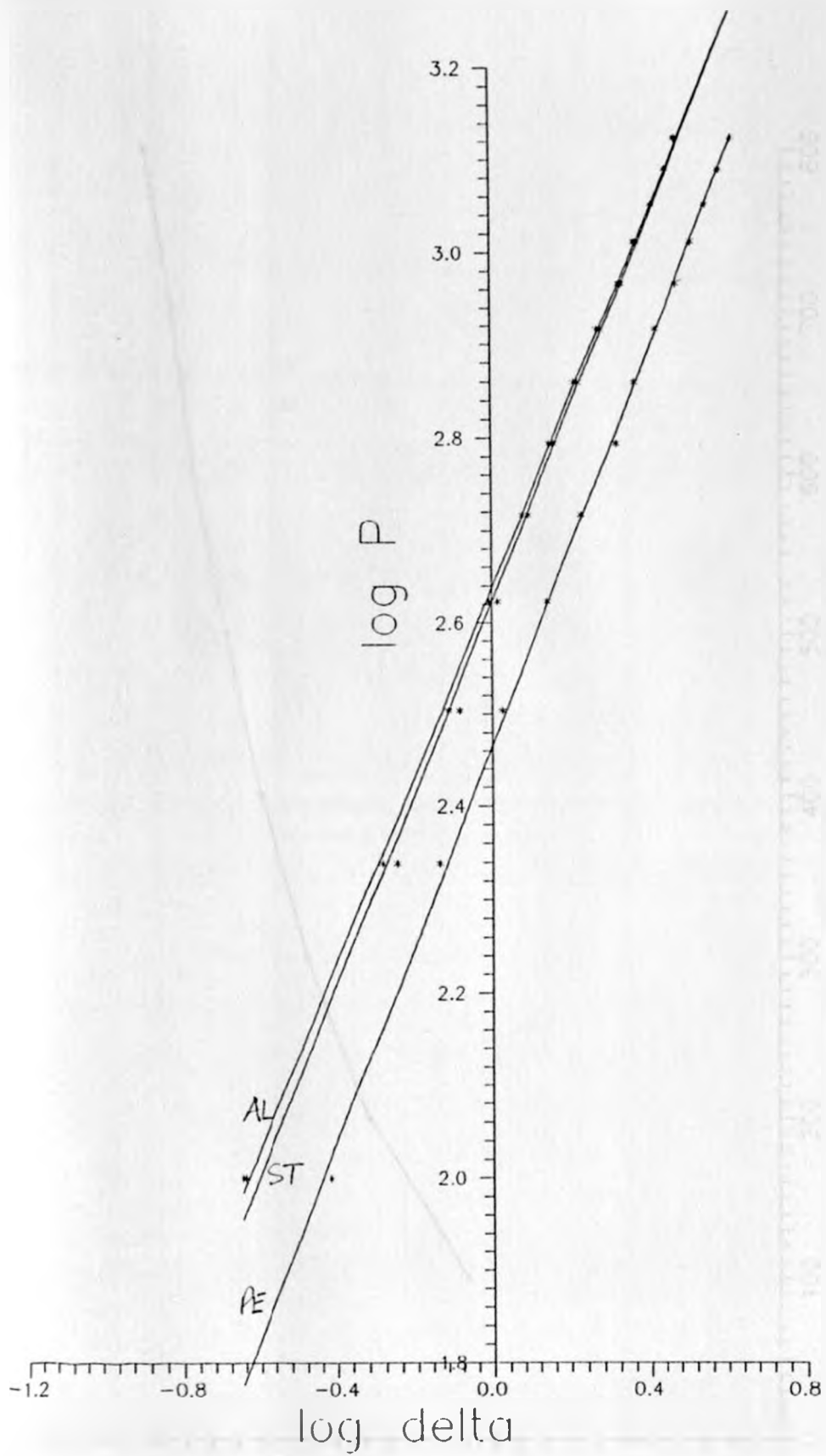


Fig. (5.1)(d) Plot of $\log P$ against $\log \delta$ for the test rollers.

73 74

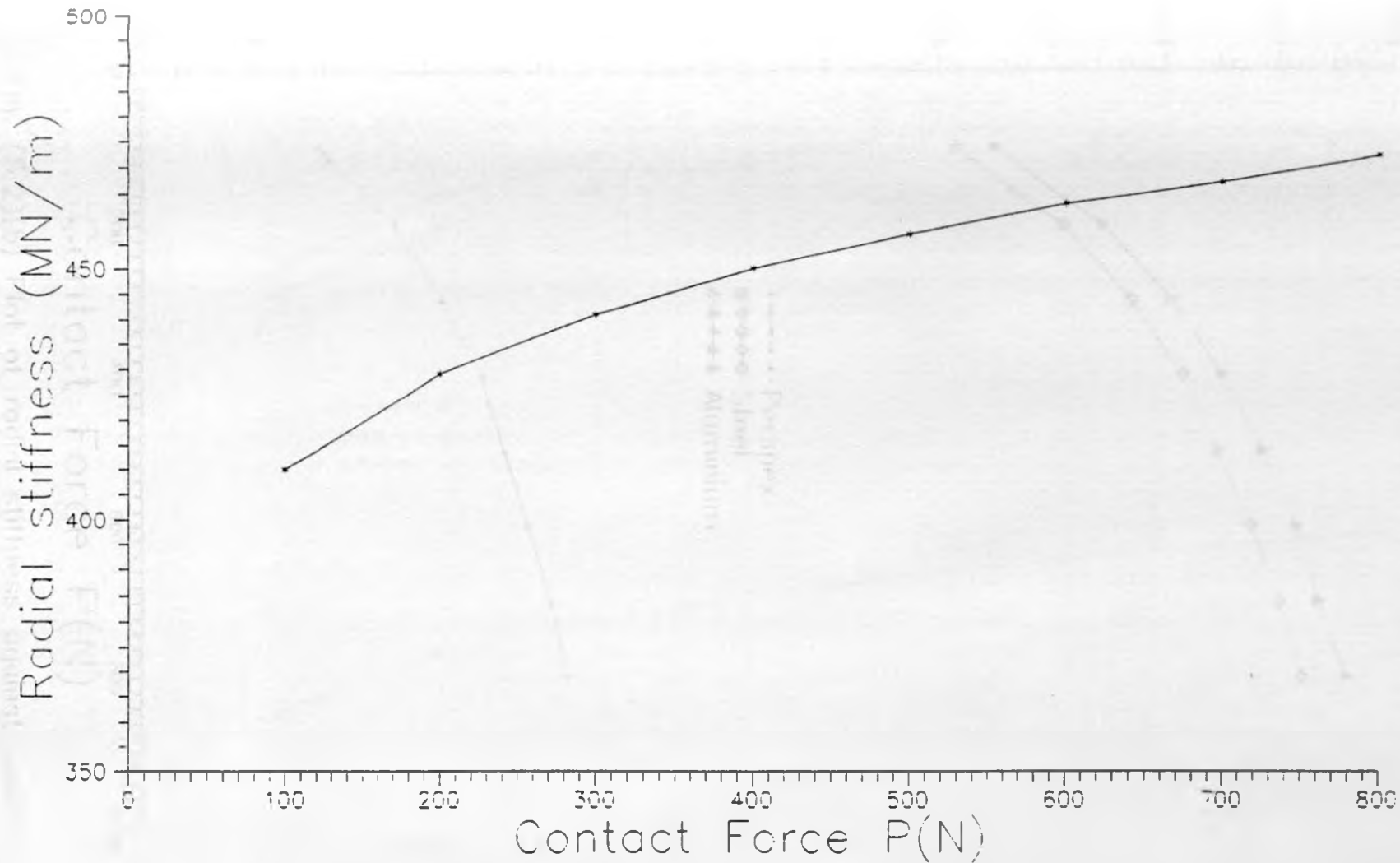


Fig. (5.2)(a) Plot of radial stiffness against contact force for aluminium.

(MN m)

480
460
440
420
400

(1) 380



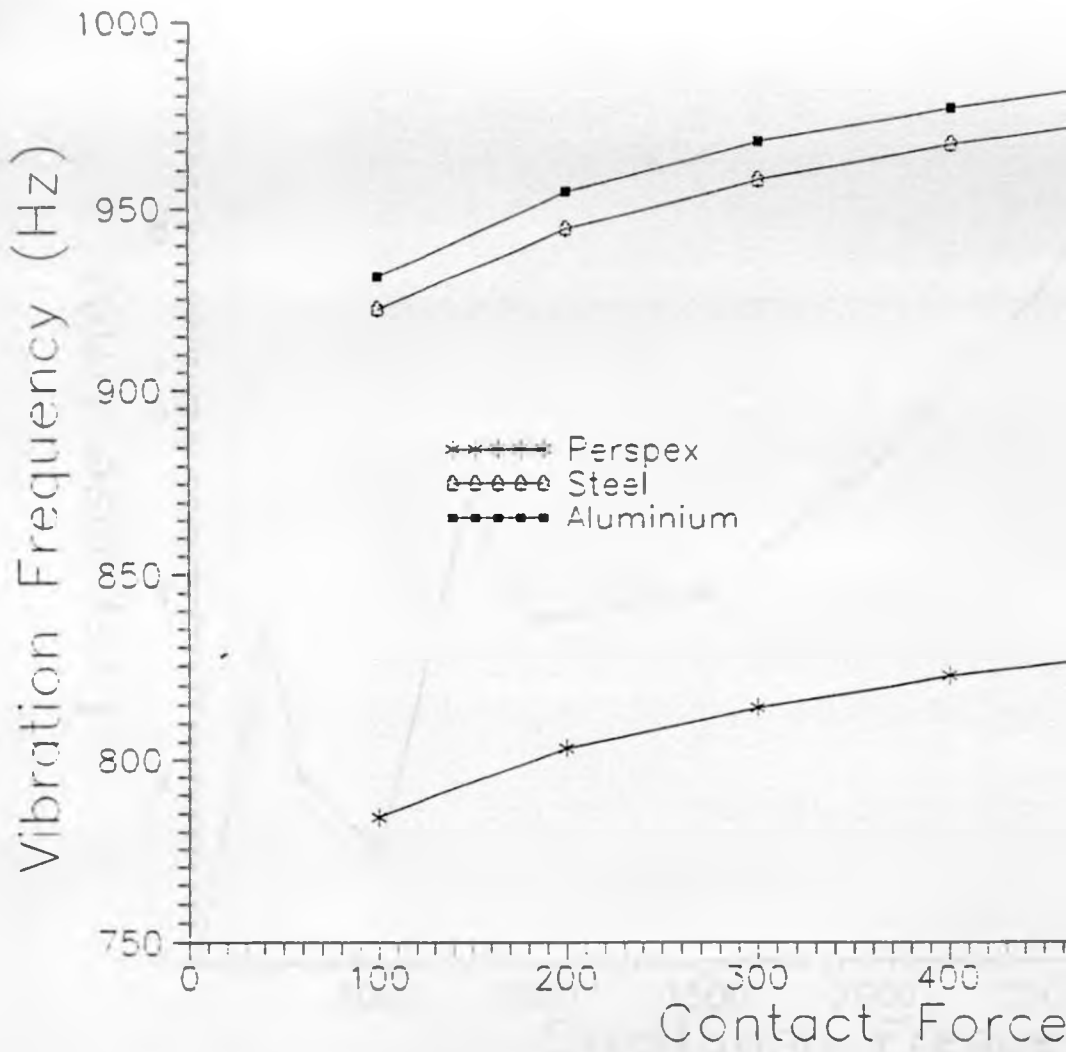


Fig. (5.3) Plot of Vibration frequency of the pivoted arm against contact force



$P(N)$

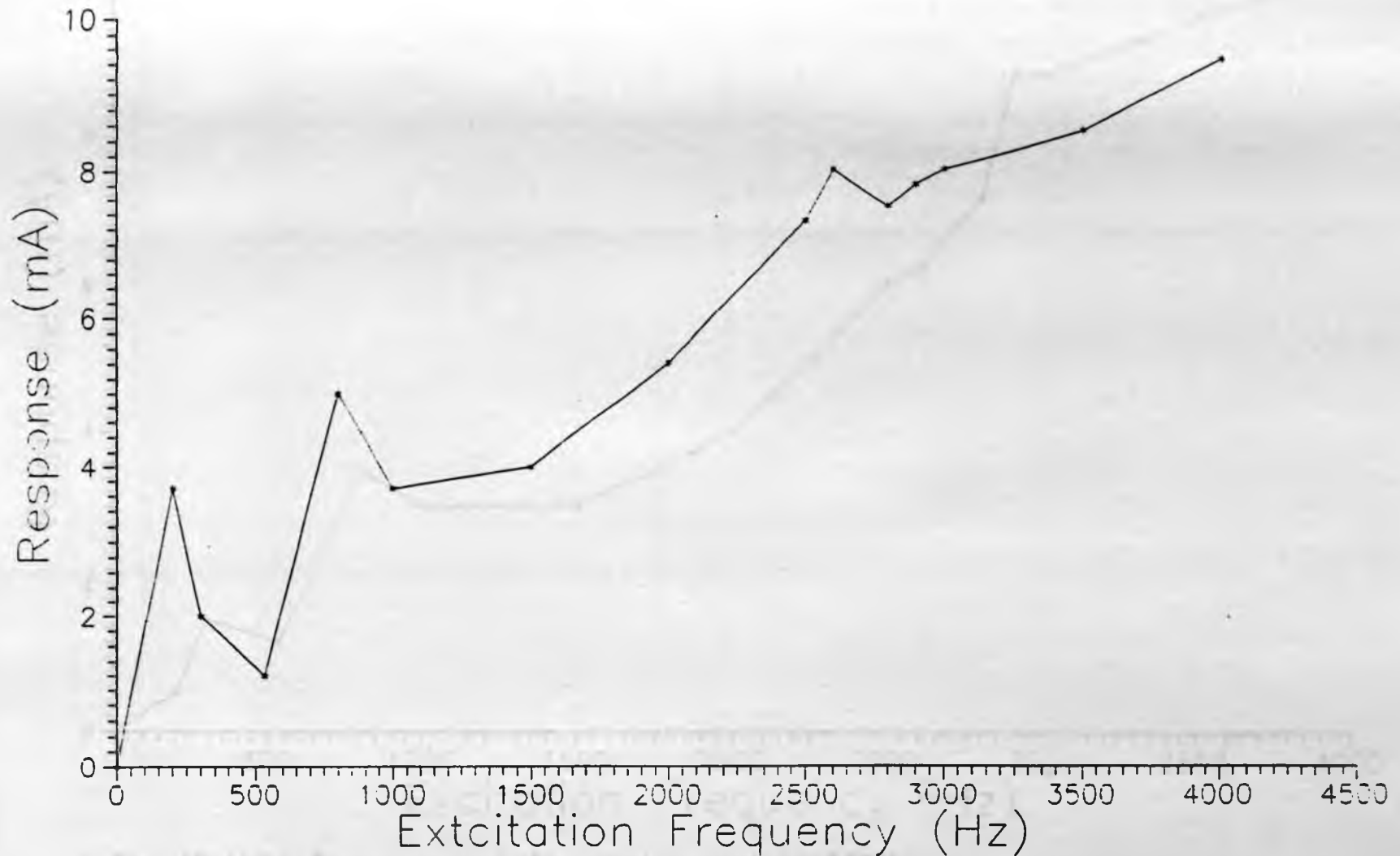


Fig. (5.4)(a) Response plot for perspex loaded at 250N

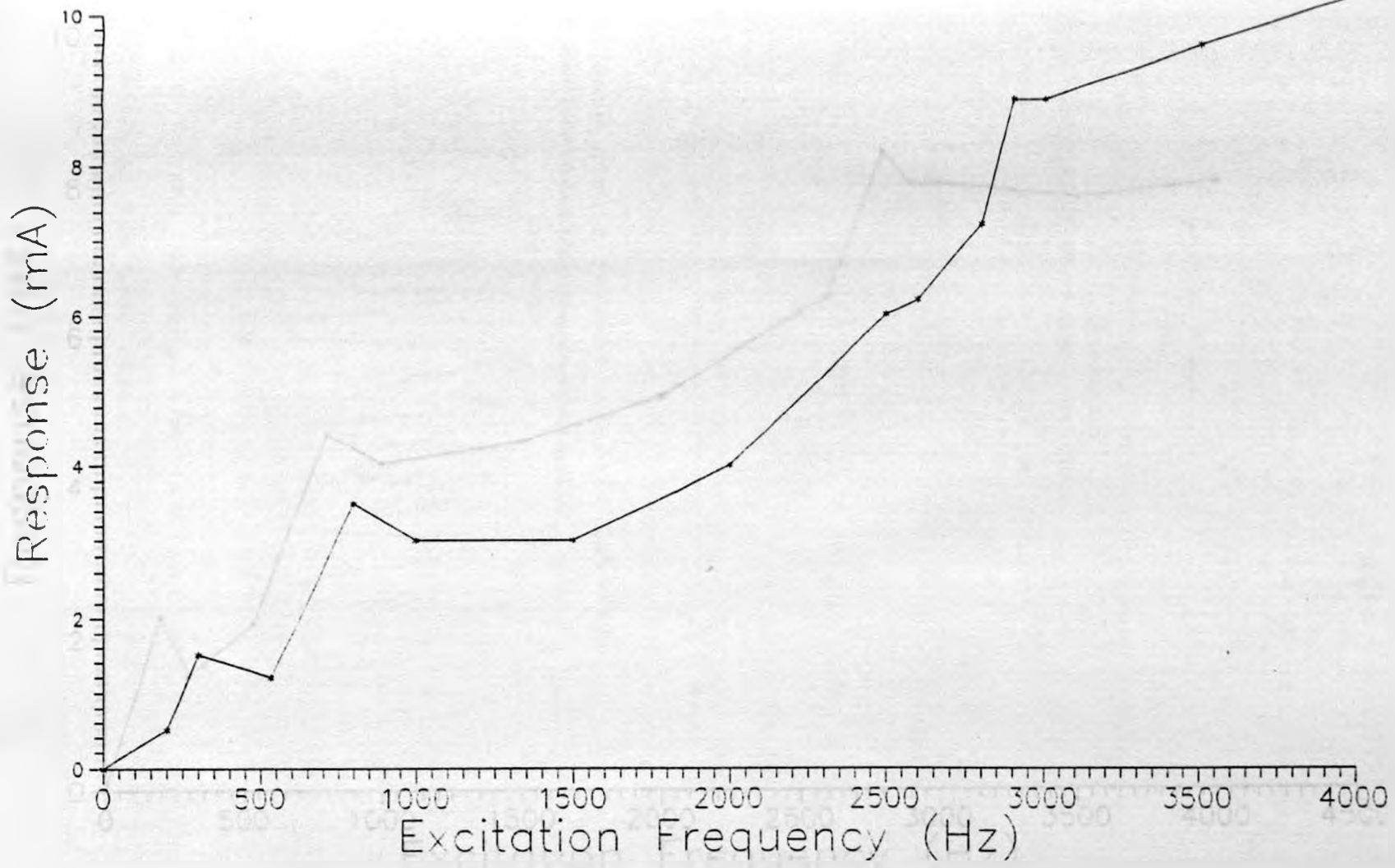


Fig. (5.4)(b) Response plot for steel loaded at 500N

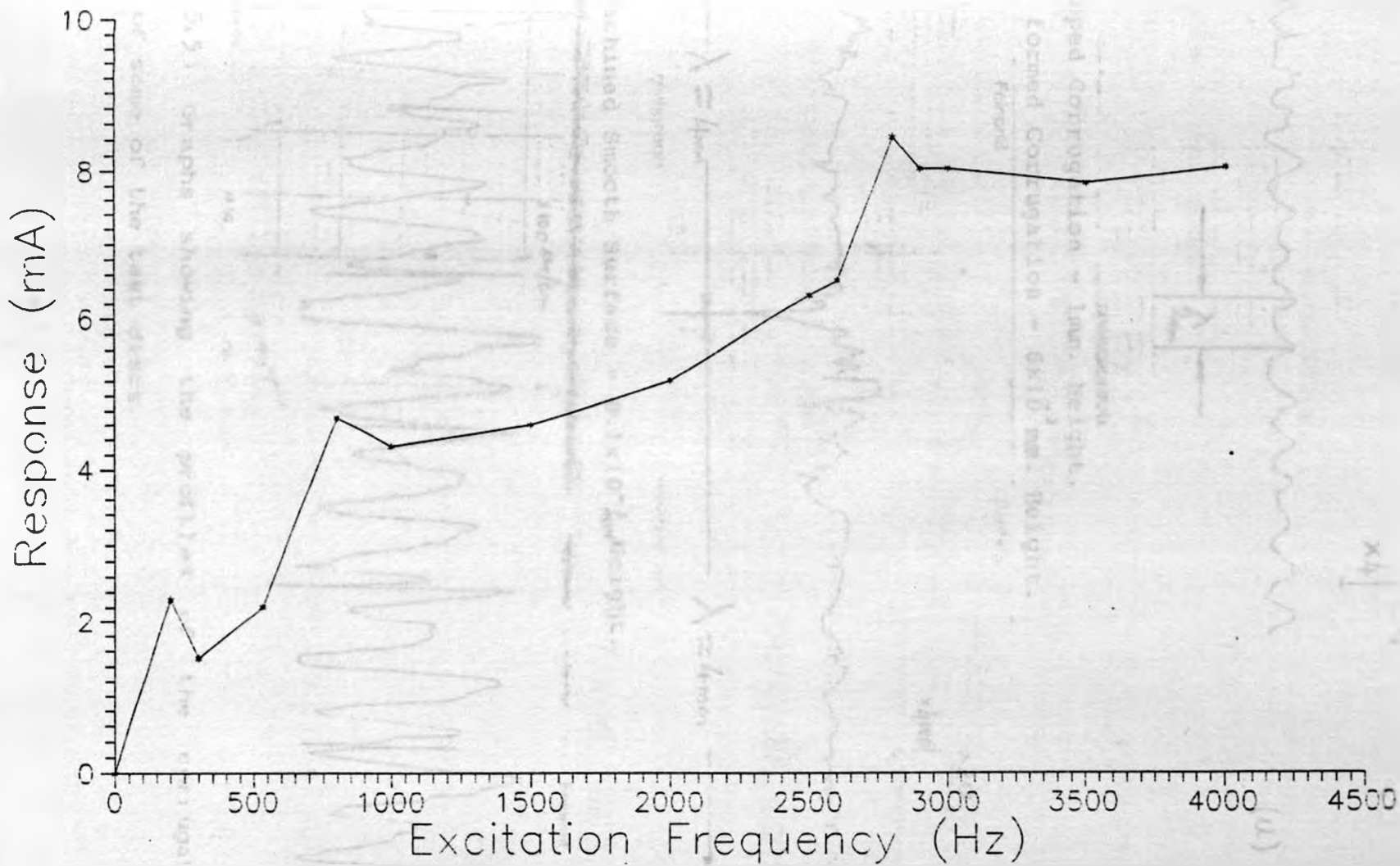


Fig. (5.4)(c) Response plot for aluminium loaded at 750N

5.8 The profiles of the corrugated surfaces

Feinprüf

Perthen

x4
x4



(a)

a). Developed Corrugation - 1mm. Height.

b). Newly formed Corrugation - 6×10^{-3} mm. Height.

Feinprüf

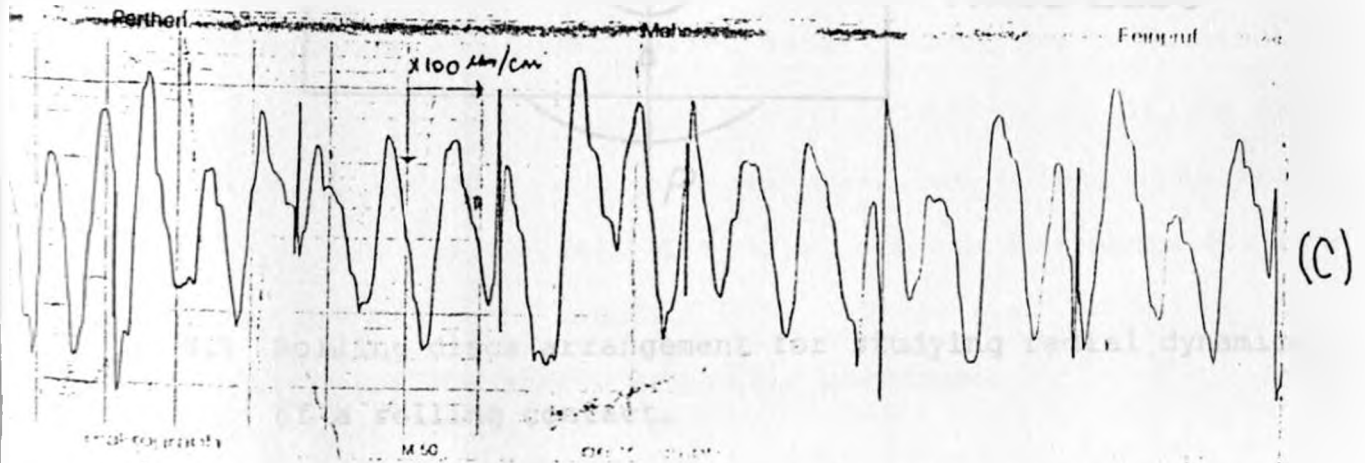
Perthen

x20
x4000



(b)

(c). Machined Smooth Surface - 0.1×10^{-3} mm Height.



(c)

Figure (5.5) Graphs showing the profiles of the corrugated surfaces of some of the test discs.

CHAPTER SIX

6. DISCUSSION

6.1 Mathematical model

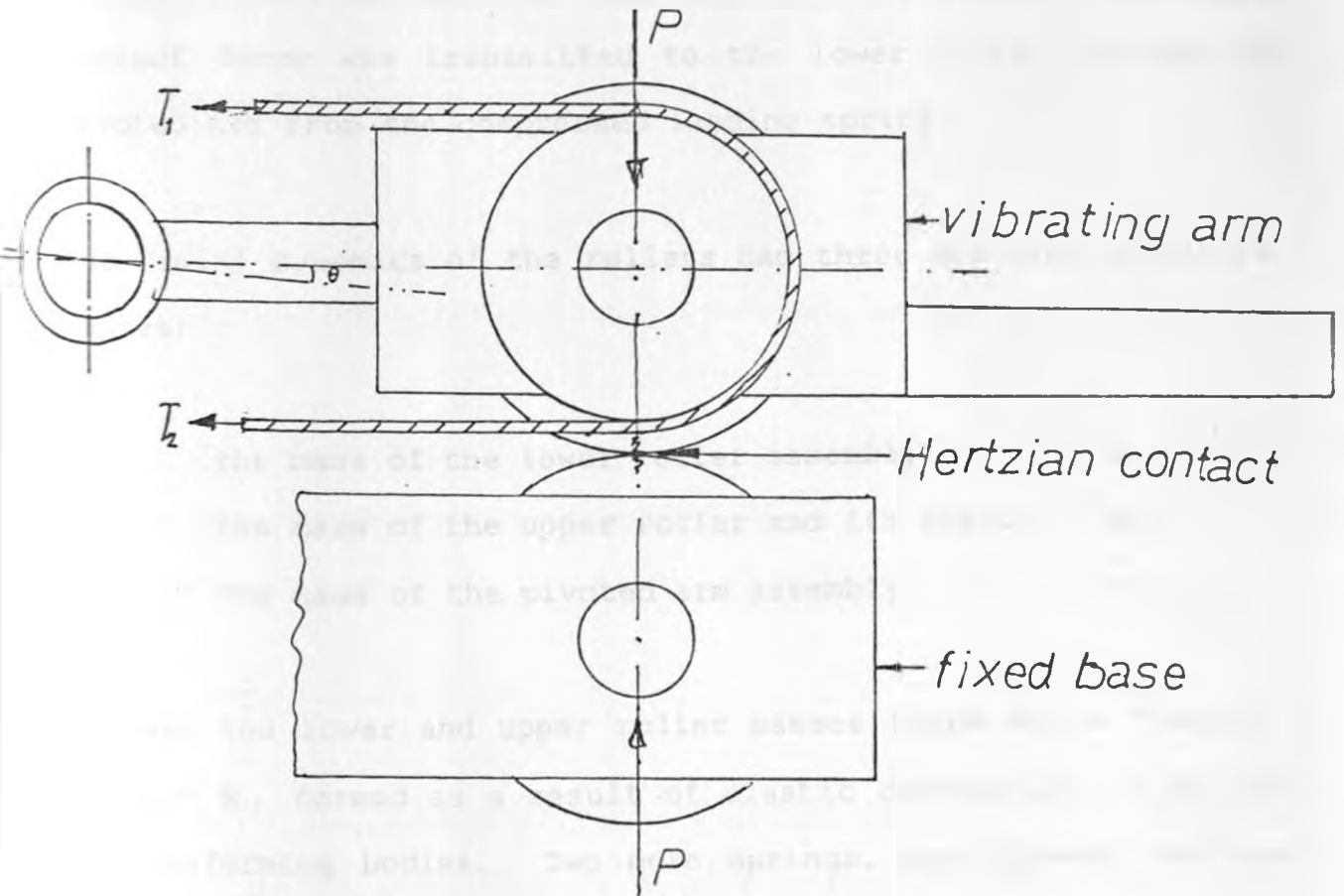


Fig. 6.1 Rolling discs arrangement for studying radial dynamics of a rolling contact.

The arrangement of apparatus shown in figure 6.1 was used to investigate the radial dynamics of a rolling contact. The lower roller rotated about an axis through the base which was dynamically fixed. The drive from the lower roller rotated the upper one due to friction. The upper roller was braked by a leather belt to vary the tangential force experienced by the contact formed between the radially loaded rollers. The radial contact force was transmitted to the lower roller through the pivoted arm from the compressed loading spring.

The radial dynamics of the rollers had three discrete effective masses;

- i) the mass of the lower roller assembly m_1
- ii) the mass of the upper roller and its shaft m_2
- iii) the mass of the pivoted arm assembly m_3

Between the lower and upper roller masses there was a "contact spring" K_2 , formed as a result of elastic deformation of the two non-conforming bodies. Two more springs, one between the base and the lower roller, K_1 , and the other between the upper roller and the pivoted arm assembly, K_3 . These two were due to flexibilities of the shafts and their bearings.

6.2 Pivoted arm resonance due to the loading spring

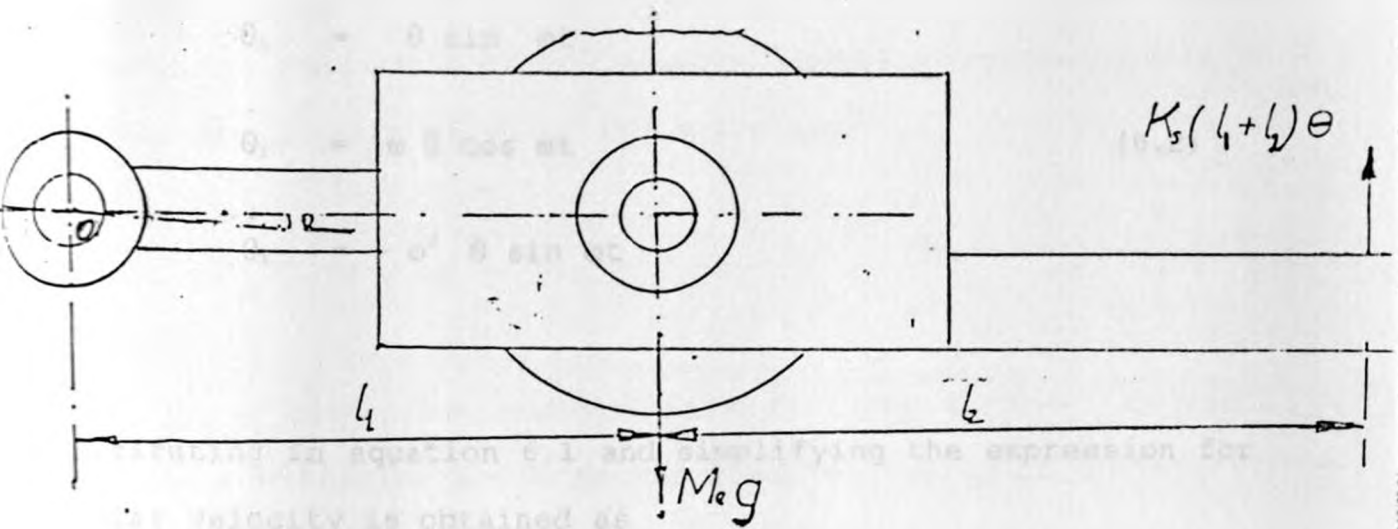


Fig. 6.2 Loading spring induced vibrations on the pivoted arm.

Figure 6.2 represents the isolated vibrations of the pivoted arm due to the compression and displacement of the loading spring. from the mean position, its equation of motion is

$$I_o \ddot{\theta} + K_s(l_1 + l_2)^2 \theta = 0 \quad (6.1)$$

where I_o is the moment of inertia of the pivoted arm about pivot point O, and is about 0.2523 Kg m^2 , and $K_s = 20.48 \text{ N/m}$ is the stiffness of the loading spring.

A harmonic motion can be assumed in which

$$\begin{aligned}\theta_i &= \theta \sin \omega t \\ \dot{\theta}_i &= \omega \theta \cos \omega t \\ \ddot{\theta}_i &= -\omega^2 \theta \sin \omega t\end{aligned}\tag{6.2}$$

Substituting in equation 6.1 and simplifying the expression for angular velocity is obtained as

$$\omega = (I_1 + I_2) \sqrt{(K_s / I_o)}\tag{6.3}$$

which numerically is 98.29 rad/sec or the pivoted arm frequency would be 15.64 Hz. This frequency is expected to give an adequate separation from the contact frequencies at approximately 900 Hz as estimated earlier in section 3.2.

6.3 Plastic deforming load estimations

Assuming a line contact to be formed initially before the toroid and the cylindrical disc are deformed by application of a radial

contact force. On the application of a contact force P , let the semi-contact width be a , as shown in figure 2.2. For such a contact the maximum contact pressure occurring in the middle of the contact zone is given by the expression

$$p_0 = 2P / \pi a = \sqrt{(P E^* / \pi R)} \quad (6.4)$$

where E^* is the plane modulus of elasticity of the contact material combination and R is the combined radius of curvature.

Because there is just a need to initiate plastic deformation the maximum contact pressure and the compressive yield stress of the softer material in the combination can be equated

$$p_0 = \sqrt{(P E^* / \pi R)} = \sigma_y \quad (6.5)$$

which gives the plastic initiating radial force as

$$P_p = \pi R \sigma_y / 50 E^* \quad (6.6)$$

for 20 mm thick rollers.

a) Steel/Aluminium combination

Here $E^* = 56.2$ GPa and since the compression yield stress of aluminium, the softer of the two, is 216 MPa it is expected that the plastic initiation load on aluminium test piece to be about 1,299.4 N.

b) Steel/Steel combination

Here $E^* = 1.0989 \times 10^{11}$ N m⁻² and with a yield stress of 250 MPa the plastic initiation load is calculated as

$$P_p = \frac{\pi * 0.025 * 250^2 * 10^{12}}{1.0989 * 10^{11} * 50} = 900 \text{ N.}$$

c) Steel / Perspex Combination

The plane modulus of elasticity is $E^* = 2.4879 \times 10^{10}$ Pa and since we expect perspex whose yield stress is 60 MPa to plastically deform first the yielding load would be 230 N.

The crowning of the steel disc has the effect of appreciably increasing the maximum contact pressure and as would be expected contact radial loads less than those calculated were found to be able to produce considerable plastic zones at the contacts. To prevent the formation of "flats" on the test pieces at loads close to the yielding values it proved appropriate to "run" , i.e., increasing the load gradually to well above the elastic limit, while the disc are rotated slowly.

6.4 Contact stiffness

When the non-conforming surfaces are parallel cylinders pressed together several simplifications occur for the Hertzian analysis as given in section 2.6. The results for plane strain loading where P is the force per unit width of contact are:

Semi-contact Width:

$$b = 2 \sqrt{[P R_1 R_2 / (R_1 + R_2)E_r]} \quad (6.7)$$

where $E_r = [(1 - \nu_1^2)/\pi E_1 + (1 - \nu_2^2)/\pi E_2]^{-1}$ is the reduced modulus of elasticity.

The elastic approach for two parallel cylinders made of the same material as given by Engel [1976] is

$$\delta = 2(1 - \nu^2)P [2/3 + \ln(4R_1/b) + \ln(4R_2/b)]/\pi E \quad (6.8)$$

It is important to note, however, that displacements and hence radial stiffness can not always be calculated, because of a logarithmic singularity in the solution. This can be physically explained by the fact that the truly two-dimensional loading of a half-space is impossible in reality. Thus, for the contact of a cylinder with a plane, the solution of this approach is indeterminate. In a given case the elastic approach and radial stiffness must then be determined experimentally as done in Sec.4.2.

Using such an approach based on equation $P = C \delta^b$ an average value of about 400 N/ μm (MN/m) for radial contact stiffness was obtained for most material pairs loaded with a contact force of 500 N and this is the value used in the subsequent analysis.

6.5 Expected contact resonance

The contact frequency will be influenced by the contact load giving rise to a particular contact stiffness, the geometry of the surfaces, the materials elastic properties, and the effective mass of the vibrating pivoted arm. Two approaches for estimating the system contact resonance in this case are:

i) Spring-mass approach

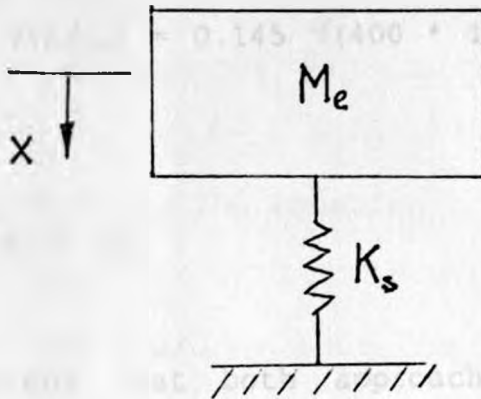


Fig. 6.3 Effective mass of the pivoted arm suspended by the contact "spring" of the Hertzian zone of rolling discs. By neglecting the loading spring effects the undamped harmonic motion of the pivot arm due to the contact "spring" stiffness lead to the angular velocity of the motion given by

$\omega = \sqrt{(K/m)} = 5773.5 \text{ rad/sec. i.e., the resonance frequency of the system is}$

$$f_n = \omega / 2\pi = 918.9 \text{ Hz.}$$

ii) Roll motion approach

Here the equation of roll motion about pivot O is as given by equation 6.1 which yields

$$\omega = 1 \sqrt{(K/I_o)} = 0.145 \sqrt{(400 * 10^6 / 0.2523)} = 5773.5 \text{ rad/sec.}$$

giving

$$f_n = 918.9 \text{ Hz.}$$

It is apparent that both approaches gives identical contact resonance in the neighbourhood of 900 Hz.

6.6 Dynamic corrugation calculations

If corrugations are formed due to plastic loading of the rolling surfaces at peak loads they will have a constant wavelength

depending upon the contact frequency and the rolling speed of the rollers.

For example the corrugations which were observed by Carson [1970] on brass discs of diameter 4 inches rolling at 150 r.p.m. and loaded at 100 lb radial force inducing a radial resonance of 500 Hz would give the following calculated parameters:

i) Corrugation wavelength

The radial contact interval period of the vibration is the reciprocal of the frequency and the peripheral displacement on the test roller during this time which gives the corrugation wavelength, is given by the equation

$$\lambda = \pi R t N/30 = \pi R N/30f_n \quad (6.9)$$

numerically this was 1.571 mm, i.e., the expected corrugation wavelength of the steel/brass disc combination loaded to produce radial vibration frequency of 500 Hz and rolled at 150 r.p.m. would be about 1.6 mm. The experimental value was 1.5 mm.

The number of peaks or troughs is given by

$$n = \frac{\text{Circumference}}{\text{Wavelength}} = 2 \pi R / \lambda = 60 f_n / N \quad (6.10)$$

For this analytical case they have to be 200 peaks and troughs.

ii) Critical speed

Analysing the previous discs combination vibrating at 500 Hz as before, the critical rolling speed of the test piece disc assuming that corrugations are formed would have been determined as follows;

Equation 6.7 gives the semi-contact width of parallel steel / brass cylinders pressed together by a contact force of 450 N per 20 mm length as

$$b = 2 \left[\frac{450 * 0.05^2 * 50}{0.10 * 2.2202 * 10^{11}} \right]^{1/2} = 0.10067 \text{ mm.}$$

Since corrugation would not form unless the expected wavelength is greater than the indentation width, i.e., $\lambda = 2 b$ at the limiting case giving

$\lambda = 2 b = \pi N_c R / 30 f_n$ hence the critical speed for this material combination loaded at 450 N is

$$N_c = 60 b f_n / \pi R \quad (6.11)$$

this means that corrugation would not form on brass disc loaded at 450 N if the rolling speed is less than 19 r.p.m. Above this speed they would be observable.

6.7 The radial vibration mode

Figure 5.8 shows the representation of the systems radial motion and a free body diagram of the system consisting of three bodies with effective masses m_1 , m_2 , and m_3 linked by three springs of stiffnesses K_1 , K_2 , and K_3 , the lower end of the first spring being fixed. The bodies can move without frictional resistance on a vertical surface. This system has three degrees of freedom in that its configuration at any instant of the time can be defined by the vertical displacements x_1 , x_2 , and x_3 of the three bodies.

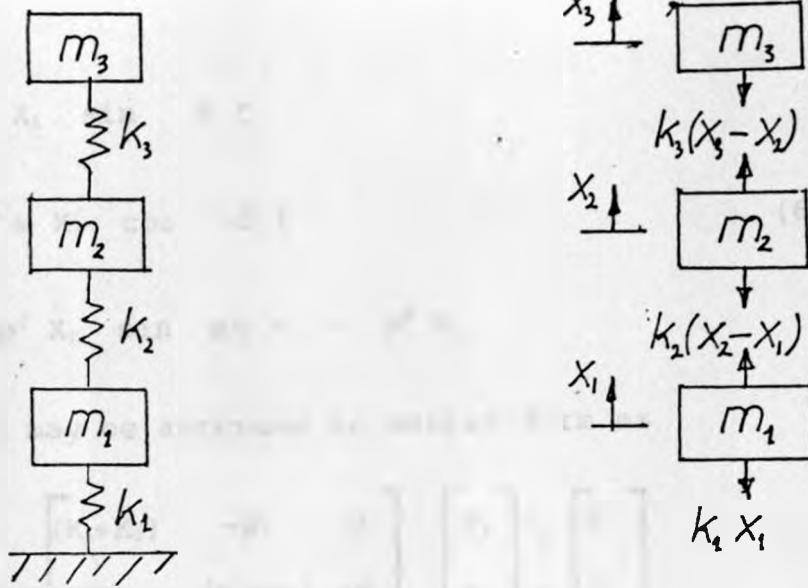


Fig. 6.4 Representation of the radial vibration of the rolling system.

The equations of motion of the three bodies are:

$$\begin{aligned}
 m_1 \ddot{x}_1 + (K_1 + K_2)x_1 - K_2 x_2 &= 0 \\
 m_2 \ddot{x}_2 - K_2 x_1 + (K_2 + K_3)x_2 - K_3 x_3 &= 0 \\
 m_3 \ddot{x}_3 - K_3 x_2 + K_3 x_3 &= 0
 \end{aligned} \tag{6.12}$$

If the bodies are disturbed from their static equilibrium positions they will oscillate freely with the same natural frequency ω . The accelerations are related to the corresponding displacements by $\ddot{x}_i = -\omega^2 x_i$, i.e., assuming harmonic motion gives

$$\begin{aligned}
 x_1 &= X_1 \sin \omega t \\
 \dot{x}_1 &= \omega X_1 \cos \omega t \\
 \ddot{x}_1 &= -\omega^2 X_1 \sin \omega t = -\omega^2 x_1
 \end{aligned}
 \tag{6.13}$$

and equation 6.13 may be arranged in matrix form as

$$\begin{bmatrix} m_1 & 0 & 0 \\ 0 & m_2 & 0 \\ 0 & 0 & m_3 \end{bmatrix} \begin{bmatrix} \ddot{x}_1 \\ \ddot{x}_2 \\ \ddot{x}_3 \end{bmatrix} + \begin{bmatrix} (K_1+K_2) & -K_2 & 0 \\ -K_2 & (K_2+K_3) & -K_3 \\ 0 & -K_3 & K_3 \end{bmatrix} \begin{bmatrix} x_1 \\ x_2 \\ x_3 \end{bmatrix} = \begin{bmatrix} 0 \\ 0 \\ 0 \end{bmatrix}
 \tag{6.14}$$

These equations can be rearranged into the required form by inverting either the mass matrix or the stiffness matrix. Owing to the diagonal form of the mass matrix however it is simpler to invert as follows

$$\omega^2 \begin{bmatrix} x_1 \\ x_2 \\ x_3 \end{bmatrix} = \begin{bmatrix} 1/m_1 & 0 & 0 \\ 0 & 1/m_2 & 0 \\ 0 & 0 & 1/m_3 \end{bmatrix} \begin{bmatrix} (K_1+K_2) & -K_2 & 0 \\ -K_2 & (K_2+K_3) & -K_3 \\ 0 & -K_3 & K_3 \end{bmatrix} \begin{bmatrix} x_1 \\ x_2 \\ x_3 \end{bmatrix}
 \tag{6.15}$$

The three eigenvalues of ω^2 provide the three natural frequencies of the system and the corresponding eigenvectors define the modes of free radial vibration. For our specific case

$m_1 = 3.5 \text{ m}$, $m_2 = 2 \text{ m}$, $m_3 = 10 \text{ m}$, $K_1 = K_3 = 0.75 \text{ K}$ and K_2 is variable depending on roller materials combination and the contact force where $m = 1 \text{ Kg}$ and $K = 10^8 \text{ N/m}$.

Rewriting equation 6.15 as

$$\begin{bmatrix} x_1 \\ x_2 \\ x_3 \end{bmatrix} = \begin{bmatrix} A_{11} & A_{12} & A_{13} \\ A_{21} & A_{22} & A_{23} \\ A_{31} & A_{32} & A_{33} \end{bmatrix} \begin{bmatrix} x_1 \\ x_2 \\ x_3 \end{bmatrix} \quad K/m \omega^2 \quad (6.16)$$

where A_{ij} takes the appropriate numerical value and from a particular eigenvalue of the coefficient matrix, the natural frequency is obtained as

$$f_n = \sqrt{\lambda_i} \cdot 10^4 / 2\pi \text{ Hz.} \quad (6.17)$$

6.8 Loading spring stiffness

Within the linear elastic range of the spring compression with the load the straight line which best represents dependence of y on x is defined as that which makes the sum of the squares of the distances from the experimental points to the line, measured in the direction of y , a minimum. According to Leaver [1974] the gradient of such a line which gives the axial stiffness of the spring is given as

$$K_s = \frac{n \sum xy - \sum x \sum y}{n \sum x^2 - (\sum x)^2} \quad (6.19)$$

From the data this becomes

$$K_s = \frac{14 (3044.125) - 126.15 * 262.5}{14 (1460.8425) - (126.15)^2} = 2.094 \text{ Kg/mm.}$$

which agrees with the previously analysed theoretical value of 1.993 Kg/mm. Experimental determination of the axial stiffness is important because work hardening and heat treatment which the springs are subjected to after manufacture can alter the mechanical properties and therefore relying on the calculated value can be misleading.

Since the total pivoted weight of the upper arm assembly is 117.6 Newtons the radial contact force on the test piece when

the loading spring of pitch 2.16 mm is tightened by n turns would be

$$P = (117.6 + 100.83 n) \quad (6.20)$$

the numerical constant 100.83 takes care of effort multiplication factor of the arm and the loading spring stiffness.

6.9 Relationship between the approach of distant points and the radial contact load

Taking the general power relationship for the approach and the contact force given by the equation

$$P = C \delta^b \quad (6.21)$$

where b is a constant dependent mostly on the solid geometry of the surfaces near the point of contact and,

C is a constant of proportionality depending on the disc material mechanical properties and the contact width.

Taking logarithms equation 6.21 becomes

$$\log P = \log C + b \log \delta \quad (6.22)$$

and the plot of $\log P$ against $\log \delta$ is a straight line of gradient equal to b and the $\log P$ intercept equal to the logarithm of constant C .

From the plots in figures 5.1 (a), (b), (c), and (d) the geometric parameter b for toroid-cylinder combination has the average value 1.073 and the material combination constants are 424, 413 and 292 for aluminium/steel, steel/steel and perspex/steel combinations respectively. The general approach-load relationships for the disc combinations are therefore

aluminium / steel	$P = 422 \delta^{1.073}$	
steel / steel	$P = 413 \delta^{1.073}$	(6.23)
perspex / steel	$P = 292 \delta^{1.073}$	

For the sphere/sphere surface contacts the general approach-load connection is as was given by equation 2.29 i.e., $P = C \delta^{1/3}$ while according to Harris [1966] for line contacts like that between a roller and the raceway of a roller bearing the approach-load relationship is

$$P = C \delta^{10/9} \quad (6.24)$$

This shows that the toroid/cylinder contact encountered in the static load-approach experiments corresponds more closely to the line contact and not the sphere/sphere point contact analysis.

Differentiation of equation 6.21 with respect to δ results in the expression for the radial stiffness within the elastic range of the deformation, i.e.,

$$K_h = \frac{dP}{d\delta} = C b \delta^{b-1} \quad \text{and since } \delta = (P/C)^{1/b} \quad \text{the}$$

stiffness expression becomes

$$K_h = C_1 P^{(b-1)/b} \quad (6.25)$$

The expressions for this stiffness in $N/\mu m$ (MN/m) for the disc combinations are therefore

Aluminium/Steel	$K_h = 300 P^{0.068}$	
Steel/Steel	$K_h = 295 P^{0.068}$	(6.26)
Perspex/Steel	$K_h = 213 P^{0.068}$	

From the graphs in figure 5.2 it is observed that there is an increase in the radial stiffness with increase in force and that

the stiffness of a perspex/steel contact is much smaller than those of the tested metal/metal contacts.

It is also observed that the calculated stiffness values based on the experimentally determined expressions are about four times higher than those which may have been calculated from the analysis of the contact made by two spheres. This is because in the theoretical analysis it was considered that the contacts are geometrically similar to the one made by two solid spheres of equal radius of curvature. Such an assumption had also been made by earlier researchers like Carson [1970] who assumed that the load-approach connection for a toroid-cylinder contact obeys the expression $P = C \delta^{1/3}$. This has been found not to be so for the line contact relationship given by equation 6.24 was found to be closer to the experimentally determined expressions.

6.10 Roll vibration of the pivoted arm due to the contact stiffness between the surfaces

The roll vibration of the pivoted arm will not only depend on the contact stiffness but also the mass of the system which in this case is the effective mass of the pivoted arm assembly. This effective mass as measured with the help of a spring balance through the contact axis is 12 Kg. The moment inertia for the assembly about pivot point o is given by the expression.

$$I_0 = m_e l^2 \quad (6.27)$$

and is numerically $I_0 = 12 * 0.145^2 = 0.2523 \text{ Kg m}^2$.

6.11 System resonances with the rollers stationary

The forced excitation and response detection of the stationary roller contacts show that for perspex / steel roller combination loaded at 250 N the response amplitude increases with the excitation frequency but there are particular frequencies at which the response is unusually higher than the neighbourhood responses. These frequencies were 200 N corresponding to the first mode of radial vibration, 800 N for the second mode and about 2,600 Hz for the third mode. These values are very close to the computed ones (266, 887, and 2,645 Hz) showing that the detected responses are indeed the systems mode frequencies.

With steel / steel roller combination loaded at a higher contact force of about 500 N there was a slight shift of the modes to higher frequencies except for the second mode which still remained at 800 Hz. The third mode was not very much identifiable as seen in figure 5.4 (b). And for aluminium / steel rollers loaded at 750 N only two modes could be easily identified. The first mode did not show up but the second and third modes occurred at 800 Hz and 2,80 Hz respectively. It

should be pointed out that a general increase of response amplitude with excitation frequency noted was due to increase in excitation energy with frequency at a constant excitation amplitude.

The experimental results show that the dynamical set up could be better assumed as a free three discrete body radial vibratory system giving rise to a number of vibration modes. The second mode (800 Hz) seem to be close to the expected pivoted arm vibration frequency but it is doubtful if these would be the ones solely responsible for the formation of corrugations because at this particular mode the two rollers represented by masses m_1 and m_2 are always on the same phase therefore creating little deformation.

6.12 General observations on the rolling tests

In all the rolling tests in which this intermittent wear was realised the rolling started smoothly but after a short period of about one minute roaring sound like that produced when a railway vehicle rolls on a corrugated track became audible in the neighbourhood of the rolling machine. Drops of lubricant did not produce any effect on this characteristic sound which was louder from steel and aluminium rollers than perspex test rollers. The commencing of the roaring sound is associated with

the initiation of intermittent wear on the rolling surfaces because in those rolling pairs in which corrugations did not develop no such sound was heard during the entire rolling period.

Intermittent wear developed within a certain radial contact force range for different material combinations. The range which shall be referred to as "the dynamic load limit" denotes the loading stress conditions which give rise to a contact stiffness coupled with an adequate peak contact stress to cause the periodic plastic deformation of the surfaces as they roll. At low loads, though radial stiffness exists, the contact force is inadequate to cause plastic deformation of the surfaces resulting in uniform wear and not corrugations. The absence of corrugations at very large contact loads is explained by the lack of elasticity at the region of contact. In the latter case rolling is accompanied by severe uniform wear of the surfaces and smoothing.

It was further observed that corrugations with constant wavelength on surfaces loaded within the dynamic range and rolled at speeds above the critical value develops initially and then flattened off with further rolling especially in the cases in which tractive forces or sliding was applied. This smearing action was less evident on steel test pieces but common on

aluminium rollers in which the high peaks were wiped off rendering the surfaces smooth. The preservation of the peaks on steel can be explained by the requirement of very high deforming blows to shape high strength steel as opposed to little force for a softer material like aluminium.

The smoothening action enhanced by the application of the tractive force is explained by the increase of the principal stresses which accompanies addition of a shearing force at the contact zone. Rolling the surfaces at higher effective contact stresses renders the zone inelastic and hence the absence of uneven wear. For corrugation formation therefore the presence of both contact elasticity and an adequate peak contact force is required.

General wear of the surfaces and especially corrugations were markedly detectable at rolling speeds above 100 r.p.m. (0.52 m/s) which is referred to as "the critical speed" for the rolling contacts. This is the speed above which the corrugation wavelength is expected to exceed the roller deformation contact width. Higher speeds of rolling surfaces with tractive forces resulted in higher wear rates because longer rubbing distance is encountered according to Archards' [1953] equation 2.2.

Finally, the most important observation made was that the intermittent wear produced on the rolling surfaces had constant wavelength dependent on the dynamical conditions of the rolling, i.e., the wavelength was proportional to the rolling speed, and inversely proportional to the radial vibration frequency. How this length is related to the dynamical parameters is discussed in detail in the following sections.

6.12.1 Corrugation wavelength and the rolling speed

It was found that between the pure rolling speeds of 100 r.p.m. (0.52 m/s) and 600 r.p.m. (3.14 m/s) the corrugations formed on the test pieces had distinct wavelengths related to the constant speed at which the driving roller was rotated. At low rolling speeds the corrugations had shorter uniform wavelengths while at higher speeds they were proportionately longer. The longer wavelengths obtained at high speeds were as a result of longer peripheral distances covered during a period of time (fixed by the systems contact frequency at a particular contact force) on rollers rotated at a faster speed than a corresponding distance on a slowly rotated one.

It should also be recalled that Harrison [1976] observed corrugations of 80 mm and 150 mm wavelength on a railway track laid on concrete slab near Glasgow. The traffic at this site

consisted mainly of passenger traffic and multiple unit (EMU) stock together with some freight traffic. The longer wavelength of 150 mm was associated with the outer rail on the curve (on which the wheels roll fast), while corrugations on the inside rail were of the shorter wavelength.

The wavelength of the corrugations formed as a result of the dynamics of the rollers in the rig would be dependent on the contact resonance, rolling speed and the diameter of the test roller and is given by the equation

$$\lambda = \frac{\pi D N}{60 f_n} \quad (6.31)$$

where

N is the roller speed in r.p.m. and D is the roller diameter.

Substituting for rollers of diameter 100 mm loaded at 700 N radial contact force results in

Aluminium	λ_a	=	N * 5.27 * 10 ⁻⁶	
Steel	λ_s	=	N * 5.32 * 10 ⁻⁶	(6.32)
Perspex	λ_p	=	N * 6.25 * 10 ⁻⁶	

The theoretical prediction of the wavelengths based on equations 6.3 was supported by the experimental results as summarised in Table 5.4.

6.12.2 Corrugation wavelength and the contact force

On the test rollers subjected to the rolling tests it was observed that the intermittent wear of constant wavelength could not form when the contact force was less than 400 N. But it readily formed when the load was between the ranges as given in Table 5.5. It was important to note that the upper load limit for the perspex / steel roller combination could not be determined within the loading capacity of the rig. Loading above the upper limits only resulted in uniform wear of the surfaces but did not produce corrugations.

It can be recalled that Kalousek [1975] reported on the severe problem of rail corrugations of long wavelength (approximately 340 mm mean) which occurred on the low rail of curves on freight lines of the Canadian Pacific Railway. It is quite obvious from investigations that the very high axle loads of approximately 300 tonnes on those lines and 400 N on the test discs was causing severe plastic deformation of the respective rolling surfaces. Since high loads increase contact stresses, and hence the probability of plastic deformation, it is apparent that the

tendency to form corrugation by gross plastic deformation would be reduced if the contact force were reduced. This explains the lack of formation of corrugations observed below the lower limit. Very high loads did not also result in intermittent wear because of lack of adequate elastic zone at the contact resulting in no periodic relaxation of the radial contact with the rolling of the surfaces which is necessary for corrugation formation.

Within the loading range in which corrugations occurred, the wavelengths did not have any direct relationship with the contact load. Just like in the case of corrugation on the rail tracks or gravel roads on which vehicles of different weights normally roll but still have constant wavelength solely dependent on the condition of the track or road, and the vehicle speeds. For example, on straight level track a distance from a station the corrugations on the tracks are normally of longer wavelengths than those at sites on a curved lines and close to stations. On the former the rail vehicles are rolled at a relatively higher speeds than the latter and since corrugation wavelength is more sensitive to the changes in speed the wavelengths differ from site to site.

Rolling steel test disc at 400 r.p.m (2.1 m/s) and loaded at different contact forces within the dynamic range in the rig

would results in corrugations whose wavelengths would be given by the equation

$$\lambda = 0.002656 P^{-0.034} \quad (6.33)$$

Table 5.6 gave the calculated corrugation wavelengths on a steel test disc rolled at 400 r.p.m. and under various contact forces based on equation 6.33. It could be seen that the corrugation wavelengths for this particular rolling speed, which is above the critical speed for the loadings, do not appreciably change with the contact force or the contact stiffness and this elucidates the experimental observations on the rolling discs and other similar observations like corrugation on the railway track whose wavelengths do not have a measurable bearing to the load but is solely dependent on the rolling speeds.

6.12.3 Rolling wear and the lateral movement

Without the lateral movement of the crowned disc there was formation of one wear track of small pits, but no corrugation developed. When the surfaces were wiped free of oil, wear was still stable and the final wear track was quite deep and smooth, with occasional pits remaining.

When the allen key was unscrewed to let the disc float with a lateral stiffness of 20,000 N/m the wear track got enlarged. Larger tracks were further obtained for 10,000 N/m and 5,000 N/m spring stiffness combinations in that order but there was no simple relation between the track widths and the lateral stiffness. With the crowned disc fully unrestricted in lateral movement a multiple number of tracks of shallow depths were formed. The results show that adverse effects of rolling wear could be best reduced by offering the rolling some little lateral movement so that the wear is evened out uniformly across the entire surface and not just restricted in a single deep track.

6.12.4 Intermittent wear and the tractive force

It was observed that the the application of a tractive force lowers the the dynamic range of all the material combinations as indicated in Table 5.5. It also results in the formation of corrugations of well defined profiles but very high tractive forces giving rise to rolling surface slip ratios above 10% caused the peaks to be flattened off as soon as they are formed.

Because higher slips necessitated by the application of large tractive forces have a tendency of increasing the shear forces

at the contact the additional of a tractive force increases the effective stress thereby enabling loads below the lower limit of the dynamic range to cause corrugations. The same argument is applicable in the case of the higher limit which is reduced as a consequence of the additional of a tractive force as the elastic portion of the contact is reduced rendering the relative radial movement of the discs impossible.

At loading conditions in which uniform wear was observed the wear rate increased with the tractive force. The effect of high tractive force as had also been observed by Wise [1987] is to increase surface-slip, friction and heat generation at the contact. This is likely to introduce thermal stresses thereby increasing the wear rate. The effects on the wear of a rolling surface due to the application of tractive forces was summarised in Table 5.7.

6.13 Corrugation and the material metallurgical properties

Mishina [1988] confirmed that the uniform wear of semi conductors is dependent on the nature of the contacting metals. The effect of the contacting metals on the friction and wear of these materials is associated with the chemical affinity and the Schottky barrier height between metal and semi conductors. Birmann [1958] also asserted that metallurgical effects are of

prime importance in determining whether corrugations do or do not form, on the superficially reasonable grounds that rail and wheel vibrations must be of secondary importance, since all rails and wheels vibrate, yet not all rails corrugate.

The scope of the study did not permit an exhaustive investigation into this phenomenon and whether metallurgical effects play a considerable part in whether or not corrugations form needs further investigations. It may however be inferred from the explained differences between aluminium, steel, and perspex test rollers which have been tested and found to corrugate under favourable dynamic conditions that metallurgical effects are not that critical in corrugation formation.

It was also important to note that examination of metallurgical differences have so far not revealed the mechanism by which corrugations form but this phenomenon alongside the study of the dynamics of rig needs further investigation.

6.14 The profiles of the corrugated surfaces

Taking figure 5.8 (a) graph as an example, the steel disc loaded at 700 N and rolled at 400 r.p.m. (2.1 m/s) is expected to have a deformed zone of width

$$2 b = 4 \left\{ \frac{P R_1 R_2}{(R_1 + R_2) E_r} \right\}^{1/2} = 0.2 \text{ mm.}$$

The theoretical corrugation wavelength as given by equation 6.32 is

$$\lambda = N \text{ (r.p.m.)} * 5.32 \text{ } \mu\text{m} = 2.13 \text{ mm}$$

which is larger than the contact width and as such it is expected that corrugations of wavelength approximately equal to 2 mm to be generated on the surface. The experimental value as can be measured from the graph is very close to that showing the accuracy of the theoretical analysis.

CHAPTER SEVEN

7. CONCLUSIONS

Previous treatment of the relationship between cylinder cylinder or toroid/cylinder approach with radial contact load as being similar to that of sphere/sphere has been found to be wanting. This is because theoretical analysis for sphere/sphere approach and contact load relationship is based on equation $P = C \delta^{1/3}$ but from the experimental results the connection should be $P = C \delta^{10/9}$. Calculation of the stiffness of toroid/cylinder based on analysis derived for sphere/sphere is therefore inaccurate.

Theoretical determination of the stiffness on cylinder/cylinder approach analysis would have been better but even with this treatment the results are only applicable for perfect plane strain loading which was not achievable in the experimental set up. It then became apparent that experimentally determined relation of approach of distant points with radial force was the only reliable method of calculating radial stiffness at any value of static load at which the contact compresses in the elastic range. Practical determination was also useful in knowing the plastic initiation

loads beyond which Hertzian analysis is impossible. This would prevent the excess loading of the disc as is encountered in the work of Carson [1970] in which a brass disc 6 mm thick was loaded at 450 N. This load according to the previous analysis is far out of the dynamic range resulting in a considerable yielded contact zone with a reduced contact stiffness and therefore invalidating the Hertzian analysis.

Corrugation is indeed a dynamical phenomenon. This is attested by the fact that all the material test pieces rolled under favourable conditions corrugated. Intermittent wear was obtained on aluminium, steel and perspex though under different dynamic conditions. Application of lubricating oil on the rolling surfaces only delayed but did not prevent the formation of corrugations. The corrugation formation and the distance between two adjacent peaks or troughs can be fully predicted from the analysis of the contact force, the surface geometries, the rolling speed and the plane elastic moduli of the bodies in rolling contact.

The corrugation wavelength is mostly affected by the rolling speed above a critical speed value. The critical speed being the minimum speed at which the rolling surfaces should be rolled so as to produce a wavelength greater than the width of the deformed zone

which in itself is load dependent. The contact load within the dynamic range has no noticeable effect on the wavelength but has a bearing on the quality of the wear profiles produced. This explains why the short length corrugation on the railway tracks differ depending on the site at which they are observed. On a straight track where the vehicles move fast the wavelength of the corrugation is longer than on a curved track or track near station at which the railway vehicle speeds are relatively low. The result tally with the observations made by Misoi [1986] who determined that road vehicles travelled faster over long wavelength corrugations on earth or gravel roads but did not give a simple relationship which relates the dynamic corrugation wavelengths to the vehicle speeds.

Application of a tractive force perpendicular to the radial force on the rolling contact greatly increases the enhances of corrugation formation at low contact loads below the lower limit of the dynamic range. This is because the introduction of a shear force increases the effective stress at the contact which enhances the formation of plastically deformed troughs as the rollers rotate. At high radial loads within the dynamic range the addition of a shear stress would cause a larger portion of the deformed zone to yield plastically, rendering the contact dynamics ineffective

in the creation of crests and troughs on the surface as the elasticity of the contact is eliminated. Further investigation to confirm this is recommended especially near railway stations at which the applications of brakes and the sliding of the wheel on the track is thought to greatly flatten out the corrugations.

Corrugation formed on a harder surface seems to resist the smearing action brought about by slip. This is because peaks of a tough material are not easily flattened down as those on a softer material hence good corrugations were retained on steel test pieces even after severe sliding motion had been introduced while on aluminium test pieces they were all wiped out. The corrugation "damping" capacity of softer materials could be useful in eliminating uneven wear on rolling surfaces where it is not needed. This would ensure smooth rolling with little disturbance to the bodies attached to the rolling surfaces.

CHAPTER EIGHT

8 RECOMMENDATIONS

Since corrugation formation on rolling surfaces is as a result of plastic deformation of an elastic contact it would be beneficial to carry further research on this phenomenon and analyse the state of stress at the contact in a three dimensional state so that the dynamic load ranges could be predicted exactly taking also into consideration the yield criteria of the softer material of the bodies in the rolling contact. It would be interesting to know whether or not tractive loads alone can produce this kind of surface wear without a normal load if the effective stress created by the former equals that brought by the latter.

Additional research work remains to be done especially in the design, manufacture and calibration of a special corrugation rig which would provide the most favourable conditions for the studying of dynamic corrugations. Determination of peak loads at various loading conditions could really help knowing the effective stress values between which corrugation formation would be a common occurrence on rolling surfaces.

9. REFERENCES

1. ARCHARD, J.F. (1953) "Contact and Rolling of Flat Surfaces" J. Appl. Phys. vol. 24 No. 8 . p. 981-988.
2. BABUS'QAQ, R.F. et al (1992) "Deformation of engineering surfaces under static loads." International Journal of Machine Tools and Manufacture. vol.32 No. 1-2 p.39-44. Pergamon Press.
3. BIRMANN, F. (1958) "Rail Corrugations; their Formation and Prevention" V.D.I. 100(16); 1253-1262.
4. BUGACIS, H. (1973) "Underground Railway tests on the Interaction between Wheel and Rails as regards Noise, Impact Transmission, Friction, Wear, and the formation of Corrugations." Transl. Leichtbau der verkehrsfahrzeuge. vol. 17 No. 5-6. p 119.
5. CARSON, R.M. (1971) "Surface Corrugations spontaneously generated in a Rolling Contact Disc Machine." Wear 17: p 59-72.

6. CARSON, R.M. (1970) "Corrugation and the Dynamics of a Rolling Contact". Churchil College Cambridge. p 71.
7. DERESIEWICZ, H. (1957) "Oblique contact of nonspherical elastic bodies". J. Appl. Mechs. 24, p.623.
8. ENGEL, P.A. (1976) "Impact Wear of Materials" Elsevier Scientific Publishing Company. p.2.
9. ENGEL, P.A. (1976) "Impact Wear of Materials". Elsevier Scientific Publishing Company. p.13-14.
10. ENGEL, P.A. (1976) "Impact Wear of Materials". Elsevier Scientific Publishing Company. p.41-42.
11. GRASSIE, S.L. (1979) "The Corrugation of Railway Track". Trinity College Cambridge. p.11-12.
12. GRASSIE, S.L. (1979) "The Corrugation of Railway Track". Trinity College, Cambridge. p.11.

13. HALLING, J. (1985) "The elastic contact of rough surfaces and its importance in the reduction of wear." Instn. of Mech. Engrs. vol.199 No. C2 p.139-144. Mech. Engineering Publications. Ltd. London.
14. HALLING, J. (1985) "The rolling resistance of surfaces covered by soft metal films." Proc. Instn. Mech. Engrs. vol. 199 No. C1 p.51-55. Mechanical Engineering Publications Ltd. London.
15. HARRISON, D. (1977) "Corrugation at Glasgow Eglinton St.: Site Report 22.03.76 and 21.11.76". Cambridge University Engineering Dept. 21 March, 1977.
16. HERTZ, H. (1886) "Miscellaneous Papers by H.Hertz." Eds. Jones and Schott. Macmillan. p 90,243.
17. HOLM, R (1946) "Electrical Contacts." Stockholm. p. 398.
18. JOHNSON, K.L. (1971) "Surface Corrugation Spontaneously Generated in a Rolling Contact Disc Machine." Wear, vol. 17. p. 59-72.

19. JOHNSON, K.L. (1972) "The dynamic response of elastic bodies in rolling contact to random roughness of their surfaces." Cambridge vol.22 No. 3 p. 323-342.
20. JOHNSON, K.L. (1985) "Contact Mechanics." Cambridge University Press. p.84.
21. KALOUSEC, J. (1975) "Measurements of Corrugated Rail Samples." Shuswap Sub-division. p 4-6.
22. KALOUSEC, J. (1975) "Track-train Dynamics." Report No.s488. p.75. Canadian Pacific Railways.
23. KRAGELSKY, V.I. (1982) "Friction and Wear, Calculation Method." Pergamon Press 1st. edn. p.237-260.
24. MATHIA, T.G. (1992) "Topograph, wear, and sliding functions of skis." Machine Tools and Manufacture. vol.32 No. 1-2. p. 263-266. Pergamon Press.
25. MEACHAN, H.C. (1964) "Transactions of the A.S.M.E." Journal of Engineering for Industry. p.808.

26. MISHINA,A.(1988) "Friction and wear of semi-conductors in sliding contact with pure metals." Tribology vol. 21 No.2 p. 76-82. Bttenworth and Co. Ltd.
27. MULVANEY,D.J.(1986) "A characterization of surface texture profiles." Proc. Instn. Mech. Engrs. vol. No.C3 p. 167-177. Mechanical Engineering Publications Ltd. London.
28. MISOI,G.K.(1986) "Vehicle Speeds on Corrugated Roads." African Journal of Science and Technology. vol. No. 1. p. 47-58.
29. NIPPON,K.K.(1978) "Ball and Roller Bearing." Nippon Tech. Div. Pr. No. 2191S. p. 80.
30. PALMGREN,A.(1956) "Ball and Roller Bearing Engineering." S.K.F. Industries. Corp. 3rd. Edn. p. 126.
31. PARKER,J.R.(1965) "Corrugation of Calender Rolls and the Barring of Newsprint." Paper Technology 6(1) p.33-41.

32. PRANCS, A. (1988) "Actual contact area growth caused by interactions of junctions in dry friction." Tribology vol. 21 No. 1. p.45-50. Butterworth and Co. Ltd.
33. SUH, N.P. (1973) "The Delamination Theory of Wear." Wear No. 25. p.111.124. Pergamon Press.
34. SMITH, I.J. (1967) "Rail and Road Corrugations." Ways and Works Branch. Dept. of Railways N.S.W. Australia Dec. 1967. p.123-142.
35. STRANG, C.D. (1952) "On the Empirical Law of Adhesive Wear." J. Appl. Phys. vol.23. No.1. p. 18-28.
36. SYMONS (1976) "Contribution to the analysis of wavyness generated during grinding." Annals of the CIRP. p.245-251.
37. WISE, S. (1987) "Railway wheelsets; a critical review." Proc. Instn. Mech. Engrs. vol. 201 No. D4 p. 257-269. Mech. Engng. Publications Ltd. London.

APPENDIX

GEOMETRY OF SMOOTH NON-CONFORMING SURFACES IN CONTACT

The profile of each body close to the origin O can be expressed:

$$z_1 = x_1^2/2R'_1 + y_1^2/2R''_1 \text{ and} \tag{A1.1}$$

$$z_2 = x_2^2/2R'_2 + y_2^2/2R''_2$$

where the directions of the axes for each body are chosen to coincide with the principal curvatures of that body. In general the two sets of axes may be inclined to each other at an arbitrary angle θ , as shown in figure (A1.1) (a).

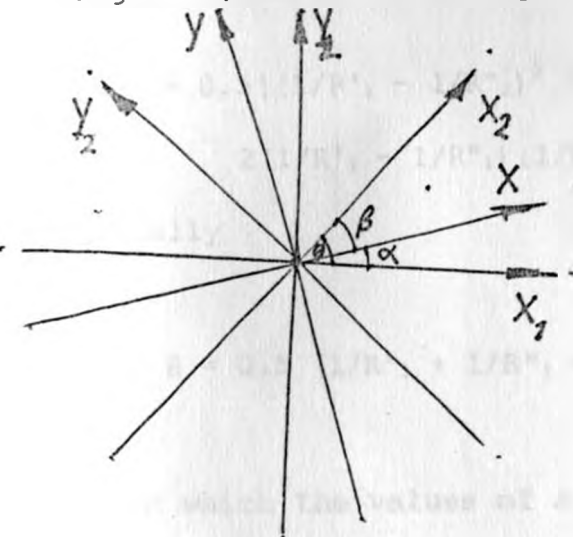


Fig. (A1.1) (a)

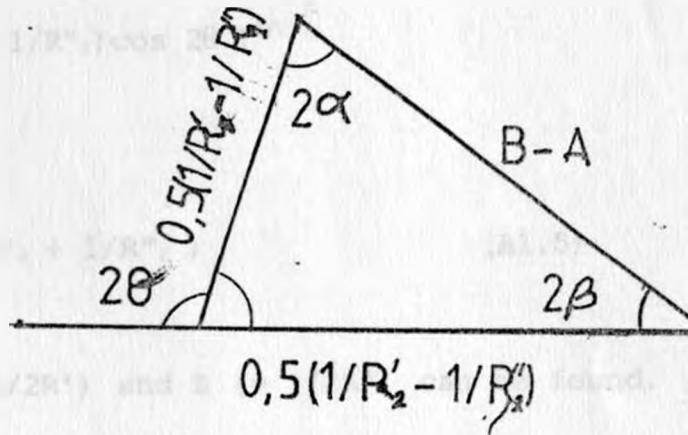


Fig. (A1.1) (b)

We now transform the coordinates to a common set of axes (x,y) inclined at α to x_1 and β to x_2 as shown. The gap between the surfaces can then be written

$$h = z_1 - z_2 = A x^2 + B y^2 + C xy \quad (A1.2)$$

where

$$C = 0.5(1/R'_2 - 1/R''_2) \sin 2\alpha - 0.5(1/R'_1 - 1/R''_1) \cos 2\alpha$$

The condition that C should vanish, so that

$$h = A x^2 + B y^2 \quad (A1.3)$$

is satisfied by the triangle shown in figure (A1.1) (b), with the results:

$$B-A = 0.5(1/R'_1 - 1/R''_1) \cos 2\alpha + 0.5(1/R'_2 - 1/R''_2) \cos 2\beta \quad (A1.4)$$

$$= 0.5[(1/R'_1 - 1/R''_2)^2 + (1/R'_2 - 1/R''_2)^2 + 2(1/R'_1 - 1/R''_1)(1/R'_2 - 1/R''_2) \cos 2\theta]^{1/2}$$

Finally

$$A + B = 0.5 (1/R'_1 + 1/R''_1 + 1/R'_2 + 1/R''_2) \quad (A1.5)$$

From which the values of A ($= 1/2R'$) and B ($= 1/2R''$) can be found.

N.B. Concave curvatures are negative.